

Monte Carlo and mean-field studies of phase evolution in concentrated surfactant solutions

Yardena Bohbot and Avinoam Ben-Shaul

*Department of Physical Chemistry and The Fritz Haber Research Center for Molecular Dynamics,
The Hebrew University, Jerusalem 91904, Israel*

Rony Granek

Department of Materials and Interfaces, The Weizmann Institute of Science, Rehovot 76100, Israel

William M. Gelbart

*Department of Chemistry and Biochemistry, University of California at Los Angeles, Los Angeles,
California 90024*

(Received 13 July 1995; accepted 16 August 1995)

A two-dimensional lattice model, originally introduced by Granek *et al.* [J. Chem. Phys. **101**, 4331 (1994)], is used to demonstrate the intricate coupling between the intramicellar interactions that determine the optimal aggregation geometry of surfactant molecules in dilute solution, and the intermicellar interactions that govern the phase behavior at higher concentrations. Three very different scenarios of self-assembly and phase evolution are analyzed in detail, based on Monte Carlo studies and theoretical interpretations involving mean-field, Landau–Ginzburg, Bethe–Peierls, and virial expansion schemes. The basic particles in the model are “unit micelles” which, due to spontaneous self-assembly or because of excluded area interactions, can fuse to form larger aggregates. These aggregates are envisaged as flat micelles composed of a bilayerlike body surrounded by a curved semitoroidal rim. The system’s Hamiltonian involves one- through four-body potentials between the unit micelles, which account for their tendency to form aggregates of different shapes, e.g., elongated vs disklike micelles. Equivalently, the configurational energy of the system is a sum of micellar self-energies involving the packing free energies of the constituent molecules in the bilayer body and in rim segments of different local curvature. The rim energy is a sum of a line tension term and a 1D curvature energy which depends on the rim spontaneous curvature and bending rigidity. Different combinations of these molecular parameters imply different optimal packing geometries and hence different self-assembly and phase behaviors. The emphasis in this paper is on systems of “curvature loving” amphiphiles which, in our model, are characterized by negative line tension. The three systems studied are: (i) A dilute solution of stable disklike micelles which, upon increasing the concentration, undergoes a first-order phase transition to a continuous bilayer with isolated hole defects. An intermediate modulated “checkerboard” phase appears under certain conditions at low temperatures. (ii) A system of unit micelles which in dilute solution tend to associate into linear micelles. These micelles are rodlike at low temperatures, becoming increasingly more flexible as the temperature increases. Upon increasing the concentration the micelles grow and undergo (in 2D) a continuous transition into nematic and “stripe” phases of long rods. At still higher concentrations the micellar stripes fuse into continuous sheets with line defects. (iii) A system in which, already in dilute solution, the micelles favor the formation of branched aggregates, analogous to the branched cylindrical micelles recently observed in certain surfactant solutions. As the concentration increases the micelles associate into networks (“gels”) composed of a mesh of linear micelles linked by “T-like” intermicellar junctions. The network may span the entire system or phase separate and coexist with a dilute micellar phase, depending on the details of the molecular packing parameters. © 1995 American Institute of Physics.

I. INTRODUCTION

The rich and diverse phase behavior of aqueous surfactant solutions is associated with the fact that the solute particles in these complex fluid systems are molecular aggregates rather than simple molecules.^{1,2} The aggregates (micelles, bilayers, vesicles, etc.) are thermodynamically stable structures, but can change their size and shape in response to changes in concentration, composition, temperature, or other ambient conditions. In all these aggregates the hydrocarbon tails of the constituent amphiphiles form a liq-

uidlike hydrophobic core while the polar headgroups are located at their surface, facing the aqueous surroundings. Consequently, in all aggregation geometries, at least one spatial dimension must be less than $2l$ where l is the length of a fully stretched amphiphile. For the three “canonical” structures—sphere, cylinder and bilayer—the number of microscopic dimensions ($\approx 2l$) is 3, 2, and 1, respectively. Most micellar aggregates can be regarded as combinations or variations of these three basic structures. For instance, a rodlike micelle is typically described as a spherocylinder,

namely, a cylinder capped by two hemispherical ends. Disk-like or ribbonlike aggregates are composed of a central bilayer body surrounded by a semitoroidal (i.e., bent, half-cylindrical) rim. Similarly, the lips of pore or line defects in bilayer sheets are also made of semitoroidal rims, but their (line) curvature is negative or zero, as compared to the positive curvature of micellar rims. A less familiar structure, which we shall feature in the present work, is that of a “T-like” (or “Y-like”) junction between cylindrical micelles, in which the local packing geometry of the amphiphiles is approximately saddlelike.

The *optimal* aggregation geometry for a given kind of amphiphile is dictated by molecular packing considerations (volume/area ratios) and their specific intermolecular interactions.³ Most double-chain phospholipids, for example, prefer the planar bilayer geometry, whereas most single-tail ionic surfactants favor packing in spherical or cylindrical micelles. The optimal micellar geometry is manifested by the shape and size of the aggregates formed in *dilute* solution, that is, in the absence of intermicellar interactions. For instance, the appearance of rodlike micelles, above the critical micelle concentration (cmc), reflects the preference of the constituent surfactants to pack in the cylindrical body. Those molecules in the hemispherical end caps involve higher packing free energy, typically a few tenths of kT/molecule, implying an excess edge free energy $\delta \approx 10$ kT per end cap.^{2,3} Linear, rodlike or wormlike, micelles are one-dimensional (1D) objects. Consequently, their size distribution in dilute solution is polydisperse with a finite average size which increases monotonically as a function of the total surfactant concentration. On the other hand, bilayers are 2D objects and their formation by monomer association involves a real first order phase transition.²⁻⁴ For instance, most lipid molecules aggregate spontaneously into extended, essentially infinite, bilayer sheets already in very dilute solution.

In this paper we shall be primarily concerned with solutions of “curvature-loving” surfactants, namely, those which in dilute solution assemble spontaneously into either globular (spherical or small disklike) micelles or into elongated cylindrical micelles. In the first case, above the cmc, when the concentration of free monomers is low and practically constant, increasing the surfactant concentration results, mainly, in the formation of additional micelles. In the second case, both the number of micelles and their size increase with concentration. Upon further increasing the concentration, intermicellar forces set in and can modify the size distribution of the micelles, their spatial ordering and even their shape. It is well known for example that at high concentrations cylindrical micelles tend to align and form hexagonal phases of rods, sometimes through an intermediate nematic phase.² This alignment can induce further micellar growth. At still higher concentrations, a transition from the hexagonal phase to a lamellar phase of bilayers can take place, due to excluded volume and/or electrostatic interactions. Such evolution demonstrates the coupling between intermicellar forces which determine the long range spatial ordering and the relatively short ranged intermolecular forces which dictate the local packing geometry.

Lamellar phases of curvature loving surfactants are

formed only at very high concentrations, where they present the most efficient way of packing large amounts of amphiphile. Upon diluting the lamellar phase pore and/or line defects will evolve in the bilayers, owing to the lower packing energy of the molecules at the semitoroidal lips of such defects.⁵⁻⁸ Eventually the hole defects will “percolate,” resulting in disintegration of the bilayer sheets into many finite (e.g., ribbonlike) micelles or in a transition into an hexagonal phase of rods.

The exact scenario of phase evolution in the concentrated solution regime depends sensitively on the interplay between the optimal packing geometry, and the interaggregate forces. Interactions between micelles whose constituent surfactant molecules do not strongly prefer, say, rod- or disklike shape, can lead to especially rich phase behaviors. Taylor, Berger, and Herzfeld⁹ have considered the particular case of no intrinsic preference for one local curvature or the other and have shown how increase in concentration can result in a succession of different micellar structures and long-range orderings: First an aligned phase of rodlike micelles appears, and then a layered state of disklike aggregates. In a related investigation, Taylor and Herzfeld¹⁰ have treated separately the situations of rod- and disk-forming surfactants, deriving in each case the sequence of isotropic-to-nematic-to-hexagonal (columnar) and smectic/lamellar states, respectively. They also examined there, for the first time, the strong coupling of micellar size to concentration and degree of ordering in the columnar and layered phases, chronicling the “growth” (and eventual divergence) of average aggregation number in the high concentration limit.

The spatial ordering in semidilute solutions of cylindrical micelles depends on the (line) *flexibility* of the micelles.¹¹ If they are rigid, a nematic or an hexagonal phase will be preferred; if they are flexible they may entangle, forming a dense solution of “living polymers.” The rigid-rod micelle work goes back to early discussions of the “sphere-to-rod” transition in isotropic phases,¹² and to treatments of the coupling of micellar size and alignment at the isotropic-to-nematic transition.^{13,14} The role of micellar flexibility in stabilizing the nematic phase has been specifically addressed by Odijk¹⁵ and more recently by van der Schoot and Cates,¹⁶ all of whom consider it to be a crucial ingredient in understanding the orientationally aligned phase. The bending flexibility of cylindrical micelles plays a perhaps still more dramatic role in explaining properties of the isotropic (even low concentration) solutions of surfactants which prefer cylindrical geometry so strongly that they form extremely long micelles just above their cmc. These systems have been shown experimentally to behave much like solutions of linear, flexible polymers, insofar as their viscosities and associated relaxation behavior are concerned.¹⁷ Their properties have been studied quite systematically in theoretical investigations which specifically exploit the polymer analogy.¹⁸

Yet another scenario is also possible. Inspired by rheological studies, several groups have recently suggested¹⁹⁻²² that certain surfactants may form *branched* cylindrical micelles, involving the above-mentioned intermicellar junctions. These predictions were most recently confirmed by direct imaging, using cryoelectron microscopy.^{23,24} The for-

mation of these structures requires special “tuning” of the spontaneous packing geometry, e.g., by changing the concentration of added salt or alcohol. Upon increasing the concentration, or lowering the temperature, the branched micelles appear to associate into connected networks, conjectured to be precursors for the formation of lamellar phases of bilayers.²⁵

In the following sections, with the aid of Monte Carlo (MC) simulations and approximate theoretical approaches, we shall analyze several different scenarios for phase evolution in self-assembling surfactant systems. Our calculations are based on a 2D lattice model which has already been used to study a limited class of systems in Ref. 1, where we have also discussed its relation to other lattice models of self-assembling systems. The formulation of this model has been motivated by experiments of Holmes and Charvolin,⁶ Boden and co-workers,²⁶ and Zasadzinski and co-workers,²⁷ on systems of surfactants whose optimal aggregation geometry is that of small oblate (disklike) micelles. These micelles persist as stable particles up to intermediate concentrations, where excluded volume interactions become significant. At these concentrations the micelles organize in a smectic-A-like phase, which upon further increase in concentration can evolve (“percolate”) into a continuous bilayer phase. Accordingly, the smallest particles in our model are disklike micelles which, upon increasing concentration, can fuse to form larger 2D structures composed of a central bilayer body surrounded by a flexible, possibly tortuous, semitoroidal rim. The micelle internal (free) energy has been expressed as a sum of a line tension term and a (line) curvature energy of the rim. The line tension, γ , measures the packing energy (per unit length) of molecules comprising an optimally curved rim, relative to their energy in the bilayerlike body. The elastic curvature energy, of the form $\kappa(c - c_0)^2$, accounts for deviations of the local (rim-) curvature c from its optimal (“spontaneous”) value c_0 , with κ denoting a 1D (rim-) bending modulus. On the square 2D lattice, this energy scheme becomes equivalent to that of an interacting lattice gas with two-, three-, and four-body interaction potentials.

Our model, albeit approximate, is quite general and allows one to examine a wide range of self-assembly phenomena, by varying its three molecular parameters, γ , κ , and c_0 . Although the model is two-dimensional it provides some important general insights into the phase behavior of 3D systems. Furthermore, even in the 3D systems, several phenomena are essentially two dimensional. These include, for instance, the transition from a smectic-A phase of disks to a continuous bilayer^{26,27} and the evolution of *defects* in bilayer lamellae.^{5–8} Surfactant monolayers adsorbed at water-air interfaces provide examples of real 2D system in which micelle formation and growth might take place. This idea has recently been invoked in order to explain monolayer pressure-area isotherms.²⁸

Our analysis in Ref. 1 focused on the special case $\gamma=0$ and $c_0=2/a$, where a is the diameter of the minimal micelle. Based on mean-field (MF) calculations we analyzed the transition from the smectic-A phase of disks to a continuous bilayer phase. Using Landau–Ginzburg (LG) analysis we in-

vestigated the possible appearance of modulated, “checkerboardlike” (CB) and “stripe” phases. Preliminary Monte Carlo (MC) simulations were also presented for one case.

Curvature-loving surfactants prefer the rim over the flat bilayer geometry and hence, in our model, can be characterized by $\gamma < 0$. In systems of this kind, on which we focus in this paper, continuous bilayers will only appear at high concentrations, due to micellar packing constraints, via fusion of “edge rich” (e.g. disk- or rodlike) micelles. Several systems, all characterized by $\gamma \leq 0$, will be studied in detail using MC simulations. The results of the simulations will be analyzed with the help of several approximate analytical approaches, which include, in addition to the MF and LG schemes, a 16-site version of the Bethe–Peierls (BP) approximation and a virial expansion (VE) approach.

In Sec. II, we outline the lattice model, comment on the MC simulations and some of the analytical approaches, and motivate the choice of systems to be studied in the following sections. The systems discussed in Secs. III–V involve solutions of surfactants characterized by different optimal packing geometries. In Sec. III, we consider a system which in dilute solution contains disklike micelles which, upon increasing the concentration, undergo an entropically driven transition to a continuous bilayer. In Sec. IV, the aggregates formed in dilute solution are linear micelles giving rise, as the concentration increases, to orientationally (nematic) and positionally ordered (stripe) phases. Finally, in Sec. V, we consider the formation of branched micelles which at high concentrations associate into connected networks.

II. MODEL

A. Hamiltonian

The 2D lattice model is illustrated in Fig. 1. The smallest particles in the system are “unit” disklike micelles of diameter D , with $a \leq D \leq a\sqrt{2}$, a denoting the lattice constant. (Hereafter, $a=1$ will be used as our unit length.) Whenever two unit micelles occupy nearest neighbor (NN) lattice sites they overlap and hence fuse to a dimer micelle. Similarly, when several micelles occupy a connected cluster of NN sites they form one larger aggregate, composed of a flat central body surrounded by a curved rim. We do not include in our model surfactant monomers whose concentration, well above the cmc, is small and constant.

Since separate micelles do not interact with each other, the total energy of a given lattice configuration is a sum of micellar “self-energies.” The self-energy of a micelle is, in turn, a sum of molecular packing free energies in its different regions, namely, the bilayer body and the curved rim. For convenience, we shall set f_b , the packing free energy per molecule in a bilayer, equal to zero. Then the micelle energy is its rim energy, which can be expressed as

$$E_{\text{rim}} = \int d\zeta \left\{ \gamma + \frac{1}{2} \kappa [c(\zeta) - c_0]^2 \right\}, \quad (1)$$

with ζ denoting the position along the micelle perimeter, $c(\zeta)$ the local (1D) rim curvature, c_0 the optimal (“spontaneous”) curvature, κ a 1D bending modulus and γ a line tension measuring the energy, per unit length, of an optimally curved

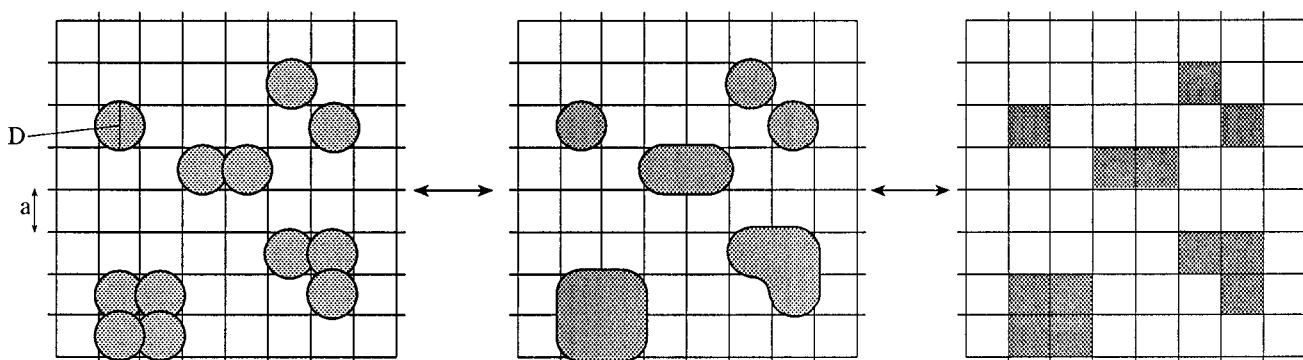


FIG. 1. Schematic illustration of the 2D-lattice model. A “minimal” (disklike) micelle occupies one lattice site (left). Micelles occupying nearest neighbor sites fuse into a larger aggregate, characterized by a flat bilayer body, surrounded by a curved rim (middle). On the square lattice (right) the local rim curvature is either straight (“flat”), or “positive” or “negative.”

rim ($c=c_0$) relative to the bilayer energy. If there are m molecules along a unit perimeter length then $\gamma=m[f_r(c_0)-f_b]$, where $f_r(c_0)$ is the packing free energy per molecule in an optimally bent rim. Depending on the molecular system considered, γ can be positive, negative or zero. In this work we shall consider the cases $\gamma=0$ and $\gamma<0$. (When $\gamma>0$ continuous, essentially infinite, bilayers are formed already in very dilute solution, as briefly discussed in Sec. III.)

On the square lattice the micelle perimeter can be represented as a sum of line segments, each of length a ($a=1$). The center of each segment coincides with one lattice vertex (four-site junction) on the rim contour. The rim segments can take one of three possible curvatures: (i) “positive,” $c_p=2/a=2$; (ii) “flat,” $c_f=0$, and (iii) “negative,” $c_n=-2/a=-2$. (More generally, we could take $c_p \neq -c_n$, e.g., $c_p=2/D$ and $c_n=-2/D'$ where D and D' denote the diameters of a unit micelle and “unit hole,” respectively.) Rim segments of unit length and different curvatures are associated with different energies (see Fig. 2). From (1) it follows directly that these energies can be expressed (ignoring constants of the order of unity) in the form

$$\epsilon_p = \gamma + (K-b)^2, \quad \epsilon_f = \gamma + b^2, \quad \epsilon_n = \gamma + (K+b)^2, \quad (2)$$

with $K = \sqrt{2\kappa}$ and $b = c_0\sqrt{\kappa}/2 = Kc_0/2$. The total rim energy is now a sum of segment energies (2), involving a sum of segment curvature energies, and a line tension contribution γL , with L denoting the total perimeter length.

The energy of a given lattice configuration can also be expressed as a sum over the four-site configurational energies, see Fig. 2. Using site occupation numbers $S_i=1$ or 0 to denote, respectively, if site i of the lattice is occupied or

vacant, let $\psi_i=(S_i, S_{i+x}, S_{i+y}, S_{i+x+y})$ denote the configuration of the four-site block in which i is the left-bottom site, $i+x$ is its NN to the right, etc. Then the system Hamiltonian can be expressed as

$$H(\{S_{ij}\}) = \sum_i \epsilon(\psi_i) = \sum_i \sum_{k=1}^4 h_i^{(k)}. \quad (3)$$

Here $\epsilon(\psi_i)$ is the energy corresponding to quartet configuration ψ_i , e.g., $\epsilon(\psi_1)=0$ where $\psi_1=(0,0,0,0)$, $\epsilon(\psi_2)=\epsilon_p$ where $\psi_2=(1,0,0,0)$, etc. [There are $2^4=16$ quartet configurations, all of which, except the fully occupied and fully vacant ones are degenerate; e.g., $\psi_3=(1,1,0,0)$ is fourfold degenerate and $\psi_4(1,0,1,0)$ is twofold degenerate.] The second equality in (3) indicates, symbolically, that the lattice Hamiltonian can be expressed as a sum of one-, two- (NN and NNN), three- (e.g., $S_i S_{i+x} S_{i+y}$), and four-body terms, corresponding to $k=1-4$. For instance the contribution to the Hamiltonian corresponding to the penultimate configuration in Fig. 2 is $S_i S_{i+x} S_{i+y} \times (1 - S_{i+x+y}) \times \epsilon_n$. The sum over i includes all M lattice sites or, equivalently, overlapping quartets. The MC simulations as well as the MF, LG, and BP approximations involved in our analysis are all based on the Hamiltonian (3).

B. MC simulations

Most of the MC simulations described in Secs. III–V were performed on 2D lattices of size $M=100 \times 100$, imposing periodic boundary conditions in the usual manner. In some cases larger lattices were used in order to examine finite size effects. Complete equilibrium of the various systems modeled was usually achieved after $\sim 10^6$ MC steps. Particle moves, of unrestricted range, were generated according to the familiar Metropolis algorithm. Both canonical (hereafter N, M, T or c, M, T ; $c=N/M$) and grand-canonical (μ, M, T) ensemble simulations were carried out. Simulations in the canonical ensemble allowed us to identify regions of coexisting phases. The grand-canonical simulations enabled to study the behavior of the chemical potential–

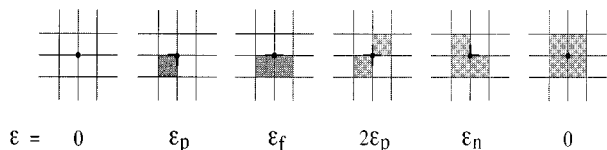


FIG. 2. Four-site (vertex) configurations and their corresponding energies [see Eq. (2)].

concentration isotherms $[\mu(c)]$, and resolve whether a given phase transition is of first order [indicated by the discontinuity of the $\mu(c)$ curves], or continuous one.

C. MF and LG approximations

The simplest (MF) approximation for calculating the system free energy, $F = E - TS$, is obtained by assigning random occupation probabilities to all lattice sites. That is, the energy $E = \langle H \rangle$ is calculated as $\langle H \rangle = M \sum_{\psi} P_0(\psi) \epsilon(\psi)$ with $P_0(\psi)$ denoting the mean-field probability of the quartet configuration ψ . For instance, $P_0(0,0,0,0) = (1-c)^4$, $P_0(1,0,0,0) = c(1-c)^3$, $P_0(1,1,0,0) = c^2(1-c)^2$, etc., where $c = \langle S \rangle$ is the fraction of occupied sites (see Fig. 2).

Using (2) and (3) to express the energies $\epsilon(\psi)$ in terms of γ , K , and b , and adding an ideal mixing entropy term, one finds for the MF free energy, per site,

$$f_0/4 = \gamma c(1-c) + c(1-c)^2(K-b)^2 + c^3(1-c)(K+b)^2 + c^2(1-c)^2 b^2 + kT [c \ln c + (1-c) \ln(1-c)], \quad (4)$$

with k denoting Boltzmann's constant and T the temperature. Note that when the 1D bending modulus, κ , is zero (hence $K=b=0$), Eq. (4) reduces to the MF free energy of a 2D lattice gas²⁹ with NN interactions $w = 2\epsilon_f - 4\epsilon_p = -2\gamma$.

In order to account for local concentration fluctuations and the possible existence of modulated phases the free energy has been expanded, beyond the MF approximation, in a LG form.¹ To this end the S_i 's appearing in the Hamiltonian (3) have been replaced by local concentration variables, $\langle S_i \rangle = c - \phi_i$ with ϕ_i denoting the local fluctuation. Then, Fourier transforming the ϕ_i 's in H (and, similarly, in the entropy contribution to F) the free energy has been expanded up to sixth order in terms of the lattice Fourier components ϕ_q . The coefficients in the expansion are functions of c and T and depend, parametrically, on γ , K , and b . The possible appearance of ordered, checkerboard and stripe, phases was examined by imposing on the ϕ_q the symmetry of these structures. This results in a LG free energy of the form¹

$$f = f_0 + \frac{1}{2} \tau e^2 + \frac{1}{4} \lambda e^4 + \frac{1}{6} \delta e^6 \quad (5)$$

with the order parameter e denoting the amplitude of the modulated phase. The coefficients τ , λ , and δ are functions of c , T and the molecular parameters γ , K , and b . Different forms of these coefficients correspond to modulated phases of different symmetries.

D. The BP scheme

The basic idea of this approach is to calculate in detail the statistical properties of a small open subsystem and treat, in a mean-field fashion, its interaction with the rest of the system.³⁰ Since our model Hamiltonian involves all possible interactions within a quartet of sites we have chosen as a subsystem a square "colony" of 4×4 sites, composed of a central quartet surrounded by 12 periphery sites; see Fig. 3. The peripheral sites are of two kinds: four "corner" (or, A -type) sites and eight "edge" (B -type) sites. The grand canonical partition function of the 4×4 (open) subsystem is³⁰

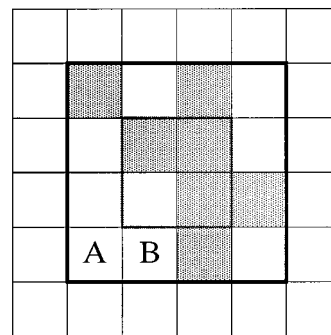


FIG. 3. The 16-site colony used in the Bethe–Peierls calculations. The grand canonical partition function [Eq. (6)] of this open subsystem is calculated by taking into account all interparticle interactions within the colony. Particles on peripheral sites also interact with the rest of the system, with different effective interactions for particles on sites A or B.

$$\Xi = \sum_{N=0}^{16} \lambda^N \sum_{\psi} \exp\{-\beta[E(N, \psi) + N_A(\psi) \phi_A + N_B(\psi) \phi_B]\}. \quad (6)$$

Here $\beta = 1/kT$ and $\lambda = \exp(\beta\mu)$ is the absolute activity (μ being the chemical potential), $E(N, \psi)$ is the energy corresponding to a colony containing N particles in configuration ψ , and ϕ_A is the effective interaction of any of the N_A particles ($0 \leq N_A \leq 4$) with its surroundings; ϕ_B , N_B , ($0 \leq N_B \leq 8$) are defined analogously.

For given temperature, T , and overall particle concentration, c , the quantities λ , ϕ_A and ϕ_B are determined by the three self-consistency equations requiring that the average occupation number of any of the four central sites, as well as that of any A and any B site, will be equal to c . That is, we require $\langle N \rangle = 16c$, $\langle N_A \rangle = 4c$ and $\langle N_B \rangle = 8c$. We calculate these averages numerically, using exact counting of all the 2^{16} possible colony configurations, with their energies calculated using (2). (Of course, many of the colony configurations are degenerate.) From these calculations we obtain chemical potential–concentration (μ – c) isotherms and pressure–concentration (π – c) isotherms. First-order phase transitions are identified by the appearance of van der Waals loops in the isotherms.

E. Systems studied

In our previous paper¹ the MF and LG schemes were applied to analyze the phase behavior of systems with $\gamma=0$. The cases considered were: $b=K$ (favoring the formation of minimal micelles in dilute solution), $b=K/3$ (larger micelles), and $b=0$ (favoring rodlike micelles in dilute solution and straight hole defects or "cracks" at high concentrations). In all three cases a first-order transition from a micellar to a bilayer phase was predicted upon increase in concentration at low enough temperature. The critical temperature T_c was found to increase with b/K . The most interesting case, $b=K$, corresponds to the transition from a smectic- A phase of disks to a lamellar phase with isolated hole defects. For this system a narrow region of a stable CB phase was predicted to exist at low T and low c .

In Sec. III, we consider again the $\gamma=0, b=K$ system, but this time using MC simulations and our BP approximation. As we shall see, these two approaches yield very similar phase diagrams. These, in turn, differ in several respects from the phase diagram predicted by the MF and LG theories, e.g., the MC simulations do not exhibit a CB phase for these molecular parameters. However, we shall see that when γ is slightly negative a stable CB phase is also observed in the MC calculations. This will be shown for the case $\gamma=-(1/2)K^2, b=K$.

In Secs. IV and V, we analyze systems with $\gamma<0, b=0$ and $\gamma<0, b<0$, respectively. In the first case, the aggregates formed at low c and low T are rodlike micelles which undergo a transition to a stripelike phase upon increasing the concentration. The analysis of this system includes, in addition to the MC and BP calculations, a virial expansion (VE) scheme outlined in Sec. IV. We shall also comment on the LG analysis of the transition from a micellar to a stripe phase. Finally, the systems considered in Sec. V exhibit the formation of branched aggregates and micellar networks. The results of the MC simulations of these systems will be interpreted based on simple qualitative considerations.

III. THE DISK TO BILAYER TRANSITION

At very low concentrations the smallest particles in the system are always preferred on entropic grounds. In our model these are the minimal micelles. When $b=K$, which is the case to be considered in this section, the minimal micelles also involve the least curvature energy, as follows from (2): $\epsilon_p = \gamma < \epsilon_f = \gamma + K^2 < \epsilon_n = \gamma + 4K^2$. The calculations presented in this section are for the case $\gamma \leq 0$.

A. MF and qualitative considerations

For the sake of comparison, we first briefly consider a system with $b=K$ and $\gamma>0$. In this case the rim energy is higher than that of a planar bilayer and a first-order transition from a dilute micellar system to a continuous bilayer sheet (with a few isolated hole and line defects) will take place below a critical temperature T_c . The MF approximation for the spinodal curve is obtained by calculating $T=T(c)$ from $\partial\mu/\partial c=0$, using $\mu=df_0/\partial c$ with f_0 given by (4). We find

$$4c(1-c) \frac{\epsilon_{\text{eff}}}{kT} = 1 \quad (7)$$

with

$$\epsilon_{\text{eff}} = 2\gamma + 4(K-b)^2 - 2b^2 - 12K^2c + 12(K^2 + 2Kb)c^2, \quad (8)$$

which, for $K=b$ yields

$$\epsilon_{\text{eff}} = 2\gamma + 2K^2(18c^2 - 6c - 1). \quad (9)$$

For an ordinary 2D lattice gas with attractive NN interactions²⁹ $K=b=0$ and $\epsilon_{\text{eff}}=2\gamma$ is the strength of the attractive potential, yielding $kT_c=2\gamma$ for the critical temperature and $c_c=1/2$ for the critical concentration. For typical bilayer forming amphiphiles such as lipids, simple molecular considerations suggest that $\gamma \geq 10$ kT at room temperatures. Thus, regardless of the value of K it follows that at room temperature a spontaneous formation of con-

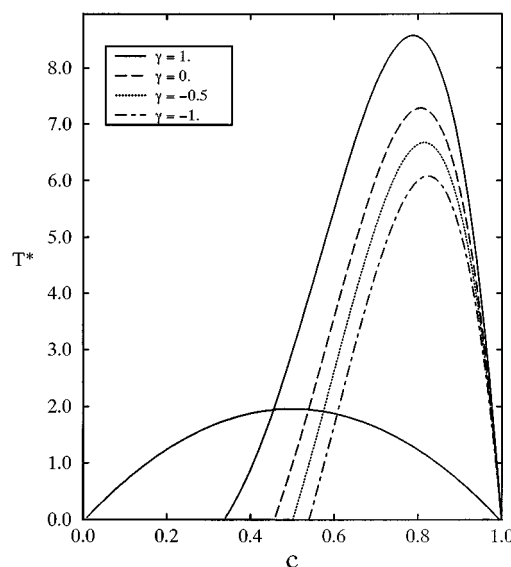


FIG. 4. Spinodal curves for the disk to bilayer transition calculated according to the mean field approximation [Eq. (7)] for $b=K$ and several values of the line tension: $\gamma=-1, 0, 0.5, 1$ (in units of K^2). $T^* \equiv kT/K^2$. For comparison we also show the (symmetric) spinodal curve, corresponding to an ordinary 2D-lattice gas with attractive nearest-neighbor interactions; this particular curve corresponds to the limiting case $K=b=0$, implying $\epsilon_p = \epsilon_f = \epsilon_n = \gamma$. For this curve $T^* \equiv kT/\delta$.

tinuous bilayers takes place at extremely low amphiphile concentrations c , as is indeed observed for lipid bilayers. The second term in (9), resulting from the curvature energy contribution (or, equivalently, from the additional two-, three-, and four-body potentials), affects the values of the critical temperature and concentration, but not the qualitative behavior of such systems.

The influence of the rim energy γ and its rigidity K on the micelle to bilayer transition are demonstrated, albeit approximately, by the MF spinodal curves, as shown in Fig. 4. The special case $K=0, b=0$, corresponding to a simple 2D lattice gas, is shown for comparison. The other curves, describing the spinodals for $b=K$ reveal the shift in c_c to higher concentrations, reflecting the resistance of the disklike micelles to fuse into bilayers. We note that the disk to bilayer transition takes place for both positive and negative values of γ and that, as expected, the critical temperature increases and the critical concentration decreases as γ increases (lower stability of the micelles). The asymmetry of the spinodal curves (with respect to $c=1/2$) can also be related to the lack of hole-particle symmetry when $b=K \neq 0$. It is easily seen, for example, that the energy change when two micelles fuse into a dimer, $\Delta E_m = 2\epsilon_f - 4\epsilon_p = -2\gamma + 2K^2$, is higher than that corresponding to hole-hole association, $\Delta E_h = 2\epsilon_f - 4\epsilon_n = -2\gamma - 6K^2$.

When $b=K$ and $\gamma \leq 0$ the minimal micelles are preferred not only entropically but also energetically over any other aggregation geometry. (The bilayer will be next on the energy scale, provided $\gamma + K^2 > 0$.) As noted above, the lower is γ , the stronger is the resistance of micelles against fusion. In the experiments of Boden and co-workers²⁶ on aqueous solutions of cesium pentadecafluorooctanoate (CsPFC), it

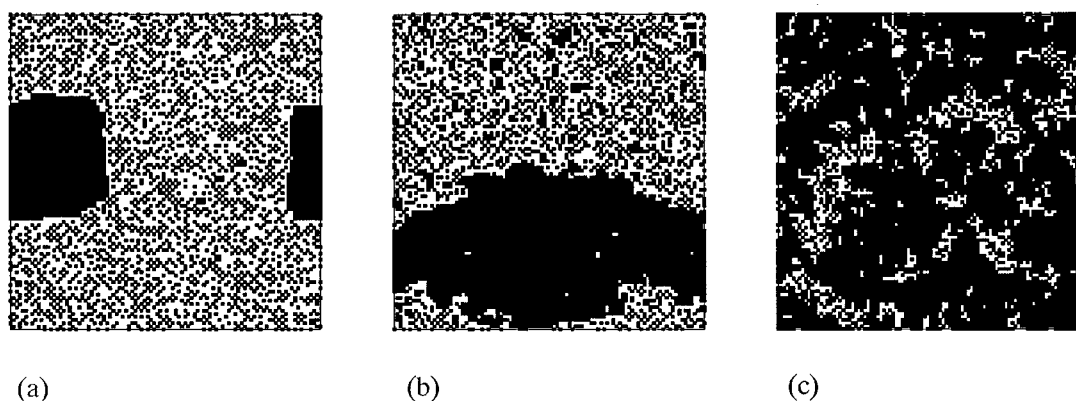


FIG. 5. The disk to bilayer transition: three typical MC snapshots corresponding to a system with $b=K$ and $\gamma=0$. (a) $T^*=kT/K^2=1.0$, $c=0.4$; at this relatively low temperature, a micellar phase of minimal disks ($c\approx 0.3$) coexists with a nearly perfect (i.e., free of hole defects) bilayer phase (see Sec. III C). (b) $T^*=2.5$, $c=0.6$; at this higher temperature the dilute phase contains larger aggregates, in addition to isolated minimal micelles. Similarly, the condensed bilayer phase contains more hole defects. (c) $T^*=3.6$, $c=0.834$; a typical configuration of the system near its critical point.

was found that small disklike micelles survive as isolated aggregates up to very high volume fractions (above 1/2). At the high concentration regime the micelles arrange in liquid crystalline, nematic and smectic-*A* phases. In other words, the micelles resemble particles in thermotropic systems. This must be attributed to the high stability of the disklike micelles, which according to our model should have $\gamma>0$. Prior to fusing into continuous bilayers (when they “run out of space”) the disks could form an ordered 2D phase. Our MC simulations for the case $b=K$, $\gamma=-(1/2)K^2$ indeed show, at low T , the appearance of a CB-like phase of disks, undergoing a first-order transition into a continuous bilayer (see below). Coexisting lamellar and disklike phases have been observed experimentally by Zasadzinski and co-workers,²⁷ suggesting that in their system (aqueous solutions of decylammonium chloride/ammonium chloride) $\gamma<0$.

The special case $\gamma=0$, $b=K$ has previously been studied using MF and LG analyses. In this system the minimal micelles and the continuous bilayer are, *energetically*, equally favorable. All other structures such as finite micelles or hole defects in bilayers involve higher energies (since their rim energies include $\epsilon_f=K^2$ and $\epsilon_n=4K^2$ contributions which are larger than ϵ_p). Since there is no energetic incentive for the micelle to bilayer transition it can only be driven by entropic or, more precisely, by packing considerations. We shall elaborate on these considerations after presenting the MC and BP calculations for this system.

B. MC and BP calculations

In Fig. 5 typical snapshots from (c, M, T) MC simulations of the $b=K$, $\gamma=0$ system, illustrate the coexistence between a micellar phase and a continuous bilayer phase. Figure 6 shows several chemical potential–concentration ($\mu-c$) isotherms, calculated by MC simulations in the μ, M, T ensemble, as well as the corresponding isotherms predicted by the BP approximation. The good agreement between the two calculation schemes is not too surprising considering the large (4×4 sites) colony used as a subsystem in the BP calculations. The BP pressure–area ($\pi-c$) isotherms were cal-

culated by numerical integration of the $\mu-c$ curves, namely, $\pi=\int c d\mu$. The phase boundaries are found as usual by comparing the chemical potentials and the pressures in the two phases. Figure 7 shows the temperature–concentration, T^*-c , phase diagram for the $b=K$, $\gamma=0$ system as obtained from the BP calculations, $T^*=kT/K^2$ denoting our reduced (dimensionless) temperature scale.

The critical temperature according to the BP approximation is $T_c^*\cong 3.65$, somewhat higher than the MC simulation value $T_c^*\lesssim 3.6$. The critical concentration is $c_c\cong 0.84$. These results, as well as the T^*-c diagram and $\mu-c$ isotherms are accurate to within a few percent, due to finite size effects in

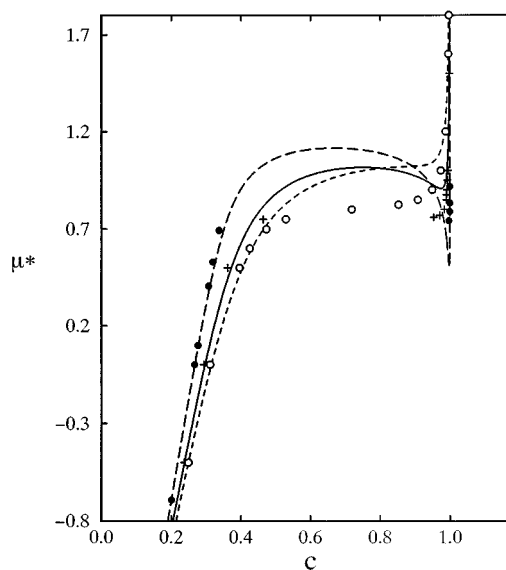


FIG. 6. Chemical potential–concentration isotherms for the $b=K$, $\gamma/K^2=0$ system; the chemical potential scale is $\mu^*=\beta\mu/K^2$. Symbols (crosses, circles) represent the results of grand canonical MC simulations; the continuous curves are calculated according to the BP approximation. $T^*=2.0$, filled circles and dot–dashed line; $T^*=3.0$, crosses and dashed line; $T^*=3.7$, open circles and solid line. Both calculations predict a similar critical temperature, $T_c^*\cong 3.6$, the MC critical temperature being slightly lower.

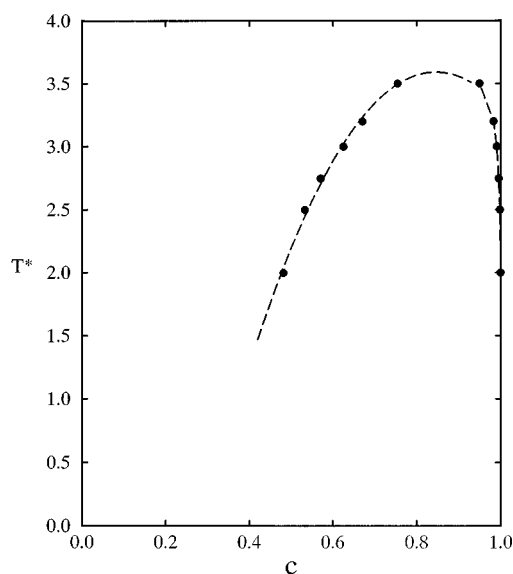


FIG. 7. Temperature-concentration phase diagram according to the BP approximation, for the system $b=K$, $\gamma=0$ (see also Figs. 5 and 6). The continuous dashed line is drawn to guide the eye. The low density branch corresponds to an isotropic phase of disklike micelles coexisting with an ordered bilayer phase which for $T^* \leq 2$ is essentially free of defects.

the MC simulations and to the limited accuracy of the numerical integration used in the BP scheme. The critical temperature obtained from the MC and BP calculations is considerably lower than that predicted by the MF analysis [Eq. (9)], $T_c^* \cong 7.45$, whereas the critical concentration predicted by the MF approximation,¹ $c_c \cong 0.81$, is quite close to the MC value cited above. The MF prediction of a high T_c^* is not surprising, considering the similar error known for the simple 2D lattice gas.²⁹

In Ref. 1 we have also presented a LG analysis to investigate the possible appearance of a modulated CB phase. It was predicted that a second-order transition from a dilute micellar phase to a CB phase should take place at $T^* \leq T_c^*/5$ with $T_c^* = 7.45$ denoting the MF critical temperature. The onset of the transition is at $c=0$ when $T^*=0$, ending up at a tricritical point (joining the micelle–bilayer transition) at $T^*/T_c^* \cong 1/5$ and $c \cong 0.22$. The simulations and BP results shown in Figs. 5–7 are at variance with these conclusions. Indeed, from Fig. 5(a) which shows a typical low temperature lattice configuration, we note the existence of short-range CB order in the system, yet no true long-range order is observed. Long-range CB order corresponds to preferential occupation of one of the two NNN sublattices of the square lattice. This, in turn, requires the appearance of an (infinite) percolation cluster on one of the sublattices. In all our simulations the transition from the micellar to the continuous bilayer took place below the percolation threshold. Several simulation runs have indeed shown a metastable CB phase at low T for concentration $c \leq 0.4$. However, this phase disappeared upon introducing a small nucleus of the bilayer phase.

On the other hand, from the qualitative analysis presented earlier in this section (Sec. III A) we can anticipate enhanced stabilization of the micellar phase against fusion when γ is negative. In other words we expect T_c^* to be lower

and c_c to be larger than their values for $\gamma \geq 0$. It is also possible that a stable intermediate ordered phase will exist at low enough temperatures. The MC simulations of the $\gamma/K^2 = -1/2$, $b=K$ system, of which typical snapshots are shown in Fig. 8, confirm these notions. Indeed, at low temperatures, the transition from the isotropic micellar phase to the continuous bilayer phase passes through an intermediate CB phase (as predicted by the LG analysis¹). Upon raising the temperature the CB phase becomes unstable, as indicated by the coexistence of the continuous bilayer and the isotropic micellar phase. The critical temperature and concentration for this system are $T_c^* \cong 3.3$, and $c_c \cong 0.85$.

C. Low T behavior

The low temperature limit of the phase diagram shown in Fig. 7, especially the *finite* concentration of the micellar phase at the transition, can be explained by the following “semi-quantitative” arguments. When $b=K$ and $T \rightarrow 0$ the minimal micelles are far more stable than any other micellar structure. These micelles can avoid fusion into larger structures by not occupying NN sites. Thus, as a first-order approximation let us assume that the system is governed by infinite NN repulsions. At very low concentrations this restriction does not severely reduce the configurational entropy of the system. As $c \rightarrow 1/2$ the micelles can still avoid fusion by occupying only sites belonging to one of the two NNN sublattices of the original lattice. However, full occupation of all the sublattice sites (at $c=1/2$) implies zero configurational entropy for the system. Thus, instead of reaching this “saturation” limit, the system may prefer to separate into two phases: a bilayer with few hole defects and a dilute ($c < 1/2$) phase consisting of micelles restricted to the sites of one sublattice. Recall that for $\gamma=0$ the fusion of micelles to form a bilayer does not involve an energetic cost (apart from edge effects), and note that the entropy per particle in the dilute phase increases as c falls below $1/2$.

More quantitatively, let c_1 and c_2 denote the densities of the micellar and bilayer phases, respectively. Assuming that the micelles are restricted to occupy the sites of only one of the two NNN sublattices, then the micellar phase can be regarded as a noninteracting lattice gas with effective concentration $2c_1$. Using the familiar equations for the chemical potential and pressure of such a system, we find²⁹

$$\beta\mu_1 = \ln[2c_1/(1-2c_1)], \quad (10)$$

$$\beta\pi_1 = -(1/2)\ln(1-2c_1). \quad (11)$$

The particle concentration in the bilayer phase is $c_2 \leq 1$. There can be only few isolated hole defects in the bilayer, since their energy, $\epsilon_h = 4\epsilon_n = 16K^2$, is very high. Thus, the bilayer can be treated as a very dilute 2D gas of noninteracting holes. The canonical partition function of a 2D system consisting of $(M-N)$ holes with “internal energy” ϵ_h , randomly distributed over the M sites of a bilayer (N being the number of particles constituting the bilayer), is $Q = [M!/(M-N)!N!] \exp[-\beta(M-N)\epsilon_h]$. The particle chemical potential and pressure in this system are easily calculated, yielding

$$\beta\mu_2 = \ln[c_2/(1-c_2)] - \beta\epsilon_h, \quad (12)$$

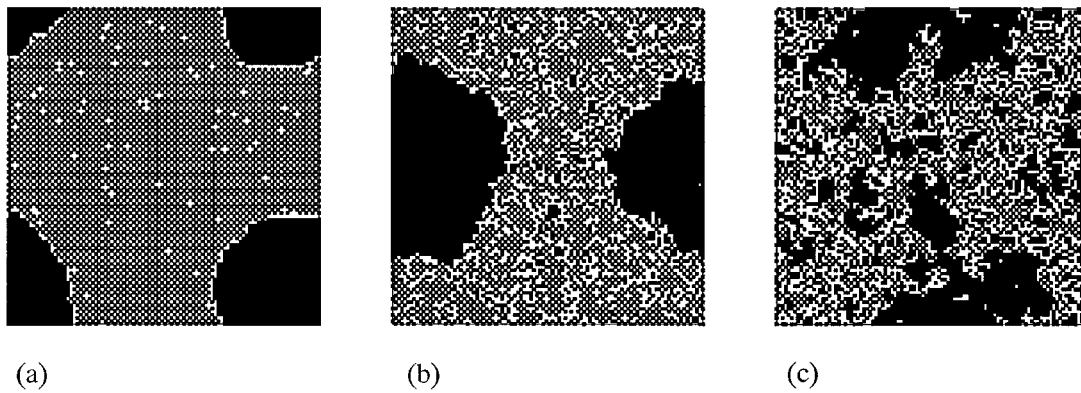


FIG. 8. Typical MC simulation snapshots for the case $b=K$, $\gamma=-0.5K^2$, illustrating the configurational changes corresponding to a change in temperature at constant concentration ($c=0.6$). (a) $T^*=1.0$, (b) $T^*=2.0$, and (c) $T^*=3.0$. At low temperatures ($T^*\leq 1.5$) a modulated checkerboardlike phase (with defects) of disklike micelles coexists with a bilayer phase. The long-range order of the micellar phase gradually disappears upon raising the temperature.

$$\beta\pi_2 = -\ln(1-c_2) - \beta\epsilon_h, \quad (13)$$

with $c_2 = N/M$ denoting the particle concentration in the bilayer.

Equating the chemical potentials and the pressures of the two phases one finds

$$4c_1^2 + 2c_1c_2^2 - c_2^2 = 0 \quad (14)$$

and

$$(1-2c_1)^{1/2} = (1-c_2)\exp(\beta\epsilon_h). \quad (15)$$

From these equations c_1 and c_2 can be evaluated numerically as a function of T . Clearly, however, as $T \rightarrow 0$ we have $c_2 \rightarrow 1$ and hence, from (14), $4c_1^2 + 2c_1 - 1 = 0$, from which we find $c_1 \approx 0.31$. Using this value in (15) it is found that for, say, $T^* = kT/K^2 = 1$ the concentration of holes in the bilayer is $\sim 10^{-7}$. In other words, the bilayer is essentially perfect, certainly on the length scale of the lattices used in our simulations.

The value found for the concentration of the dilute phase at coexistence with the bilayer (at $T \rightarrow 0$) is just slightly lower than the value estimated from the simulations, $c_2 \approx 0.33$. The difference can be attributed to our assumption that the micelles in the dilute phase are strictly restricted to only one sublattice. Locally, as we see in Fig. 5(a), the micelles preferentially occupy one of the two sublattices but, globally, both sublattices are equally populated. Differently put, the fact that we have not observed true long-range CB order in our simulations indicates that the effective concentration on any of the two sublattices must be less than 0.59, the value corresponding to the site-percolation threshold for the 2D square lattice.³¹ The possibility of observing this behavior at very low temperatures (lower than the lowest temperature in the simulations, $T^*=0.5$) cannot be ruled out. However, at these low temperatures finite size effects can play a significant role in determining the fine details of the phase transition. (Note for example that the condensed phase at very low T appears as a finite perfect domain, free of hole defects, whereas it is obvious that such defects should appear at any nonzero temperature.) Alternatively, as we have seen in Fig. 8, true long-range order is easily established once the mi-

celles are even slightly further stabilized, namely by having γ slightly negative.

IV. LINEAR MICELLES, STRIPES, AND DEFECTS

In this section we consider the phase behavior of a system in which the preferred aggregation geometry in dilute solution is that of straight linear micelles, analogous to cylindrical micelles in 3D systems. In our model such systems are characterized by vanishing spontaneous curvature of the micellar rims, i.e., $b=0$, and negative rim energy, $\gamma < 0$, ensuring lower packing energy in the (straight) rim compared to the bilayer body: $\epsilon_f = \gamma < \epsilon_b \equiv 0$. Since $b=0$ we have $\epsilon_p = \epsilon_n = \gamma + K^2$, implying particle-hole symmetry of the system free energy, around $c=1/2$. Thus, for instance, in complete analogy to the growth of linear micelles with increasing concentration in the dilute solution regime^{2-4,12} ($c \geq 0$), we expect the growth of line defects upon dilution in the high concentration regime⁸ ($c \leq 1$). We shall be mostly concerned here with intermediate concentrations, where intermicellar (interhole) interactions can influence micelle (hole) size, and induce the formation of orientationally and translationally ordered phases.

A. Energetics

To ensure that the flat bilayer is the least favorable aggregation geometry we require $\epsilon_f < \epsilon_p = \epsilon_n < \epsilon_b = 0$, implying $-\gamma > K^2$. Furthermore, to ensure linear micellar growth in dilute solution we require that the end cap energy of a straight linear micelle will be positive. In general, the internal energy of a linear micelle is of the form $E_s = \alpha s + \delta$ with s denoting the aggregation number, or the length of the aggregate measured in some suitable units.^{2,3,32} In our model a linear micelle of size s is composed of a string of s (fused) unit micelles, for which

$$E_s = 2(s-1)\epsilon_f + 4\epsilon_p = \alpha s + \delta, \quad (16)$$

where $\alpha = 2\epsilon_f = 2\gamma$ and

$$\delta = 4\epsilon_p - 2\epsilon_f = 2(\gamma + 2K^2) \quad (17)$$

with the second equality following from (2).

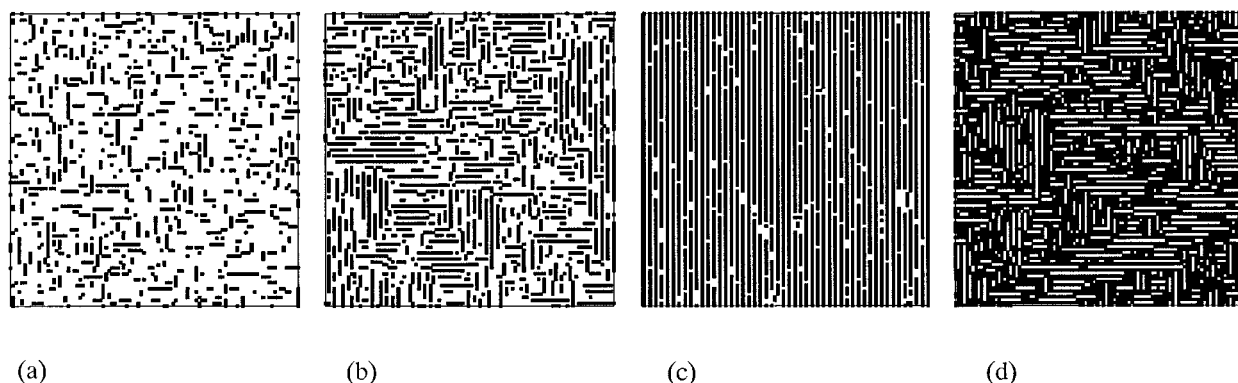


FIG. 9. Typical MC snapshots illustrating the phase evolution in the $b=0$, $\gamma=-1.5K^2$ system, upon increasing the concentration at constant temperature, $T^*=0.3$. The concentrations corresponding to configurations a, \dots, d are, respectively, $c=0.15, 0.30, 0.46, 0.70$. (a) At moderately low densities the system consists of relatively short and isotropically oriented rodlike micelles. (b) At $c \approx 0.3$ long-range orientational order sets in, inducing further micellar growth and ultimately the formation of an ordered, stripe, phase. (c) A stripe phase consisting of very long rods with few hole defects. At this temperature when $c=0.5$, the system is a perfect modulated stripe phase. (d) Above $c=0.5$, particles and holes exchange roles, due to the particle-hole symmetry of this system.

When $\delta > 0$ the association of two micelles into a longer one is energetically favorable, $E_s + E_{s'} - E_{s+s'} = \delta > 0$. Thus $\delta > 0$ enhances micellar growth. In ordinary micellar solutions the weight average micelle size in dilute solution increases with concentration according to $\langle s \rangle \approx 2\sqrt{c \exp(\delta/kT)}$. A similar behavior is expected in our model (see below), the fact that our linear micelles are embedded in a 2D rather than a 3D medium being irrelevant.

Combining our two requirements, (i) $\epsilon_f < \epsilon_p = \epsilon_n < \epsilon_b = 0$ and (ii) $\delta = 4\epsilon_p - 2\epsilon_f > 0$, we find using (2), $1 < -\gamma/K^2 < 2$. Accordingly, in the numerical calculations presented in this section we have used $-\gamma/K^2 = 1.5$, implying $\delta = K^2$ and $\epsilon_f = -1.5K^2$, $\epsilon_p = \epsilon_n = -0.5K^2$. The phase diagram corresponding to this case is very different from that of the system considered in the previous section ($b=K$, $\gamma \neq 0$). First, as noted above, it is symmetric around $c=1/2$. Second, consistent with the qualitative arguments given above regarding the requirement $1 < -\gamma/K^2$, our MC simulations confirm that a phase transition from a dilute micellar phase to a condensed bilayer phase, indeed, does not take place in this system. This conclusion is also consistent with the predictions of our approximate MF theory. More explicitly, from (8) we find that for $b=0$, $\gamma/K^2 = -1.5$ the effective pair interaction energy is $\epsilon_{\text{eff}} = -K^2[12c(1-c) - 1]$. Hence, except at very low or very high values of c ($|c| < 0.092$) the spinodal curve corresponds to $T < 0$. [Two ‘‘critical points’’ are predicted by (7), at $c \approx 0.04$ and 0.96 with very low critical temperatures, $T_c^* = kT_c/K^2 \approx 0.08$. These should be regarded as artifacts of the MF approximation.]

The absence of a condensation transition does not exclude the possibility of phase transitions from the isotropic micellar phase to orientationally and/or spatially ordered phases. In fact, since at low temperatures, the predominant aggregation geometry is that of linear rodlike micelles we expect the appearance of an isotropic-nematic phase transition. This conclusion is, indeed, corroborated by our MC simulations, as well as by a virial expansion treatment of the system free energy. Both approaches predict a second-order phase transition.

A LG analysis of the $b=0$, $\gamma/K^2 = -1.5$ system predicts

a phase transition from the isotropic micellar phase (or isotropic phase of hole defects in the bilayer) into a spatially modulated stripelike phase at $T^* \leq 1.23$. The appearance of a stripe phase at intermediate concentrations (and $T^* \leq 0.86$) is confirmed by our MC calculations. However, the LG analysis (to which we return at the end of this section) also predicts that the transition from the isotropic to the stripe phase is of first order at high T^* ($0.45 \leq T^* \leq 1.23$) and of second order at lower temperatures. On the other hand, the MC simulations indicate a second-order transition at all T . Recall, however, that at low T a transition to an orientationally ordered phase can also take place. Based on the MC simulations our conclusion is that orientational order sets in prior to positional order, so that the transition to the stripe phase actually occurs from the nematic (rather than from the isotropic) phase. We shall further elaborate on this issue in the following discussion.

B. MC and BP calculations

Figures 9 and 10 show two series of MC snapshots obtained from c, M, T and μ, M, T simulations. Figure 9 illustrates the progression of phases upon increasing the concentration, at a relatively low temperature $T^* = kT/K^2 = 0.3$. At low c the system consists of a dilute isotropic phase of rods [Fig. 9(a)]. As c increases, still in the isotropic phase, the rods grow and form aligned domains [Fig. 9(b)]. Then, over a short concentration range, the system develops into a stripe phase characterized by long range orientational and translational order [Fig. 9(c)]. Finally, when $c > 1/2$ the stripes fuse to a continuous sheet with line defects [Fig. 9(d)]. Note the particle-hole symmetry, as reflected by Fig. 9(b) ($c=0.3$) and Fig. 9(d) ($c=0.7$).

Figure 10 describes the transition from the high T isotropic phase to the low T anisotropic stripe phase upon lowering T^* at constant concentration, $c=1/2$. The stripe phase appears at $T^* \approx 0.86$. It should be noted that $T^* = kT/K^2$ can be varied by changing either T or K . In real surfactant solutions the bending rigidity (K) can be tuned by varying, for

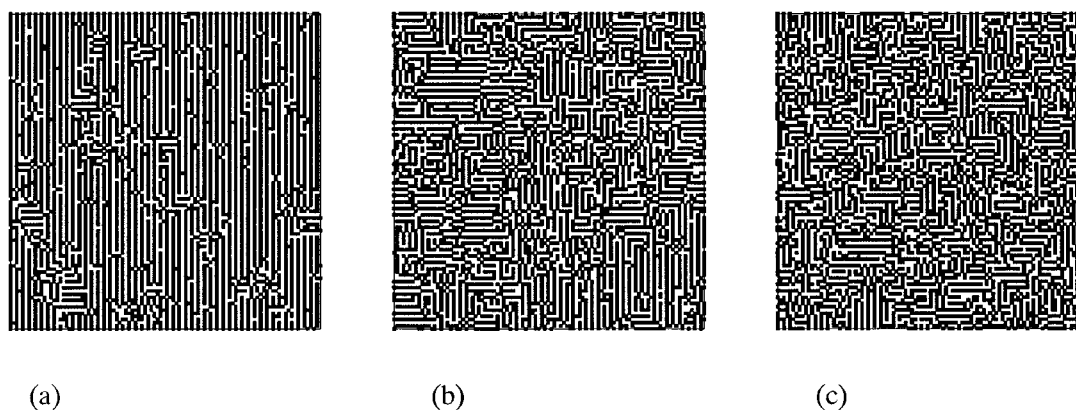


FIG. 10. Typical MC simulation snapshots of the system $b=0$, $\gamma=-1.5K^2$. Here the concentration is held constant at $c=0.5$, and the temperature is lowered across the isotropic-stripe phase transition. Configurations *a*, *b*, and *c* correspond, respectively, to $T^*=0.84$, 0.85 , and 0.9 . Above $T^*\approx 0.86$ the order parameter, η , as defined in Eq. (18) vanishes, indicating the loss of orientational order.

instance, the salt concentration (in ionic systems) or by adding a cosurfactant.

Figure 11 shows two sets of μ - c isotherms, one calculated based on the BP approximation and the other evaluated from MC simulations in the μ, M, T ensemble. The isotherms are continuous but show (between $c=0$ and 0.5 and then between $c=0.5$ and 1) changes in slope, involving flat regions which narrow down as T^* increases. The MC simulations did not show separate $\mu(c)$ branches and we thus conclude that the transition from the isotropic to the orientationally anisotropic (nematic or stripe) phase is not of first order. Consistent with this conclusion, the BP isotherms are monotonic, i.e., not showing van der Waals-like loops. It

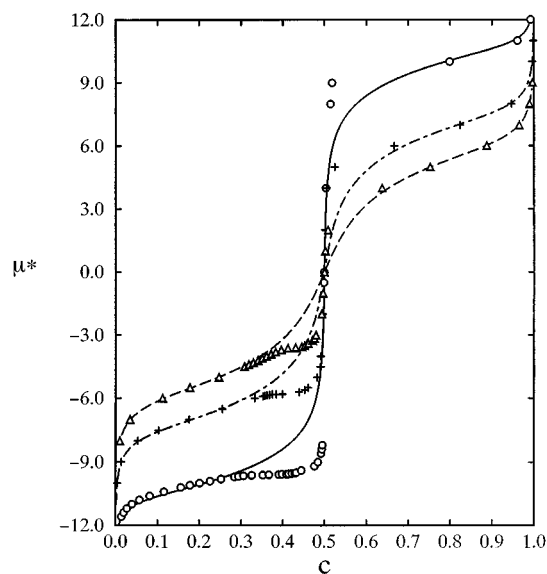


FIG. 11. Chemical potential-concentration isotherms for the $b=0$, $\gamma=-1.5K^2$ system, $\mu^*\equiv\beta\mu/k^2$. Shown are the results of grand canonical MC simulations (symbols) and calculations based on the BP approximation (continuous curves): $T^*=0.30$, open circles and solid line; 0.45 , crosses and dot-dashed line; 0.60 , triangles and dashed line. The change in slope of the MC isotherms which, for the above three temperatures, takes place at $\tilde{c}\approx 0.31$, 0.36 , 0.41 , marks the transition from an isotropic to an orientationally ordered phase of rodlike micelles.

must be noted however that the BP scheme is not expected to be accurate once the typical rod size exceeds any of the linear dimensions of the open subsystem; namely, four lattice sites in our present calculations, see Fig. 3. This typically happens at the concentration corresponding to the onset of the isotropic-anisotropic transition, beyond which the rods begin to grow rapidly. It is not surprising that at these concentrations the BP isotherms start deviating from the ones derived from MC simulations, as seen in Fig. 11.

To characterize the isotropic-anisotropic transition in a more quantitative fashion we define an orientational order parameter, $\eta=\eta(c, T)$, in terms of the (thermally averaged) numbers $n(x)$ and $n(y)$ of “bonds” between NN pairs (of fused unit micelles) along the x and y directions of the square 2D lattice:

$$\eta = \frac{|n(x) - n(y)|}{n(x) + n(y)}. \quad (18)$$

This order parameter, which ranges between 0 and 1, measures the extent of orientational anisotropy of the system: $\eta=0$ for an isotropic system and $\eta=1$ for a system of rodlike micelles or stripes, all pointing along the x or the y direction. Figure 12(a) shows the variation of η between $c=0$ and 0.5 for the two temperatures, $T^*=0.3$ and 0.45 , corresponding to the two MC isotherms shown in Fig. 11. The calculations show that $\eta=0$ up to a critical concentration $c=\tilde{c}(T^*)$ above which it increases sharply, but continuously with c . For the two temperatures considered, $\tilde{c}\approx 0.31$ and 0.37 for $T^*=0.3$ and 0.45 , respectively. The values of $\tilde{c}(T^*)$ coincide with the points in Fig. 11 where the μ - c isotherms change their slope. Our calculations also reveal that the increase in η beyond \tilde{c} is accompanied, as expected, by a sharp increase in the average size of the rodlike micelles. In Fig. 12(b) we show the change in η with T^* at $c=0.5$, corresponding to the simulations shown in Fig. 10. Again we note a sharp, but continuous, increase in η as T^* falls below 0.86 , marking the transition from an isotropic to a stripe phase.

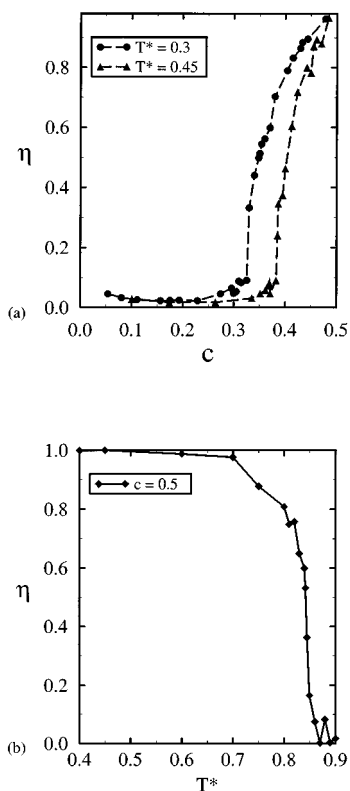


FIG. 12. (a) MC calculations of the orientational order parameter, η , as a function of concentration, c , for the system considered in Fig. 9, for the two temperatures $T^* = 0.30$ and 0.45 . (b) Order parameter η vs T^* for $c = 0.5$, corresponding to the system in Fig. 10. The sharp increase in η below $T^* \approx 0.86$ indicates the appearance of an orientationally ordered stripe phase.

C. Low T behavior: VE analysis

The increase of \tilde{c} with T is a reflection of the intricate interplay between micellar growth and intermicellar interactions. In the model system analyzed here, the predominant aggregates at low T and low c are rodlike micelles. It is easily seen that the energetic penalties, ΔE , of forming other structures, such as “ T -like” junctions between two perpendicular micelles, or a “ L -like” bend in a linear micelle, increase sharply as T decreases; hence, their statistical weights decrease exponentially with $\Delta E/kT$. (For these two examples $\Delta E_T/kT = [2\epsilon_n - (2\epsilon_f + 2\epsilon_p)]/kT = 3/T^*$ and $\Delta E_L = [(\epsilon_p + \epsilon_n) - 2\epsilon_f]/kT = 2/T^*$, respectively, where we have used $\epsilon_f = -1.5K^2$, $\epsilon_p = \epsilon_n = -0.5K^2$.) On the other hand, as noted earlier, linear association of rodlike micelles is a favorable process, with $\Delta E/kT = -\delta/kT = -1/T^*$ implying a (weight) average micelle size which, in dilute solution, scales as $\langle s \rangle \sim \sqrt{c} \exp(\delta/kT) = \sqrt{c} \exp(1/T^*)$. At low T and c the micelles are rodlike, interacting via excluded area repulsions. The average excluded area per particle, v , is of order $\langle s \rangle^2$ (see below) while the average density of rods is $\rho = c/\langle s \rangle$. The isotropic–anisotropic transition is expected to occur when $\rho = \tilde{\rho} = \tilde{c}/\langle s \rangle \sim 1/v$, implying $\tilde{c} \sim \langle s \rangle^{-1}$ or, for our specific system, $\tilde{c} \sim \exp(-1/2T^*)$. This simple and familiar scaling argument explains the decrease of \tilde{c} with T at low temperatures (when the micelles are predominantly rodlike), but it does not indicate whether the transition is of first or higher

order. We now turn to a somewhat more quantitative analysis of the low T and c regime of the phase diagram, based on a virial expansion of the system free energy.

Suppose T is sufficiently low that all the micelles are linear rodlike aggregates, possibly touching each other, thus forming (with small probability) T - or L -like junctions; see Fig. 9. Let $\rho_s(\Omega)$ denote the density of rods of size s and orientation Ω . In our 2D square lattice model $\Omega = x$ or y . The number of unit micelles associated into s, Ω rods is $N_s(\Omega) = s\rho_s(\Omega)M$ where M is again the area of the system (total number of sites). Then, clearly

$$\sum_{s, \Omega} s\rho_s(\Omega) = c. \quad (19)$$

For a given size-orientation distribution of rods $\{\rho_s(\Omega)\}$, the Helmholtz free energy of the system, F , including intermicellar interactions in the second virial approximation, is given by

$$\frac{\beta F}{M} = \sum_{s, \Omega} \rho_s(\Omega) \left(\ln \rho_s(\Omega) - 1 + \beta E_s + \sum_{s', \Omega'} \rho_{s'}(\Omega') B_{ss'}(\Omega, \Omega') \right) + \rho_1 \ln 2. \quad (20)$$

Here E_s denotes the energy of an s, Ω micelle (which is independent of Ω) as given by (16), and

$$B_{ss'}(\Omega, \Omega') = -\frac{1}{2M} \int d\mathbf{r} d\mathbf{r}' \times \{ \exp[-\beta U_{ss'}(\mathbf{r}, \Omega; \mathbf{r}', \Omega')] - 1 \} \quad (21)$$

is the contribution to the second virial coefficient of the system from interactions between rods of size s and s' with given orientations Ω and Ω' , respectively. $U_{ss'}(\mathbf{r}, \Omega; \mathbf{r}', \Omega')$ = $U_{ss'}(|\mathbf{r} - \mathbf{r}'|, \gamma)$ denotes the total interaction potential between the rods, including both excluded volume and “self” (rim) energy contributions (see below); $\gamma = \gamma(\Omega, \Omega')$ is the angle between the two rods. In our lattice model the integration over \mathbf{r}, \mathbf{r}' is replaced by lattice summation.

The first two terms in the sum in (20) represent the “mixing” entropy of the system, with rods in different orientations treated as distinct species. Writing $\rho_s(\Omega) = \rho_s f_s(\Omega)$ with $f_s(\Omega)$ denoting the normalized orientational distribution of s rods one can rewrite the entropy as $\sum_s \rho_s [\ln \rho_s - 1 + \sum_{\Omega} f_s(\Omega) \ln f_s(\Omega)]$ thus separating the size-polydispersity and orientational contributions to the entropy. The third term, $\sum_s \rho_s(\Omega) E_s$, is the internal (“chemical”) energy of the system and the last term in the sum accounts for intermicellar interactions. The summation over s extends from $s = 1$ to ∞ ; the last term in (20) corrects for the fact that unit micelles ($s = 1$) do not involve orientational entropy, i.e., $\rho_1(x) = \rho_1(y) = \rho_1/2$ and hence their contribution to the entropy is simply $\rho_1(\ln \rho_1 - 1)$.

The equilibrium distribution $\{\rho_s(\Omega)\}_{\text{eq}}$ is found by minimizing (20) subject to the conservation condition (19), yielding the self-consistency equations

$$\rho_s(\Omega) = \frac{1}{2} g_s \lambda^s \exp\left(-\beta\delta - 2 \sum_{s'\Omega'} \rho_{s'}(\Omega') B_{ss'}(\Omega, \Omega')\right), \quad (22)$$

with $g_s=2$ for all $s \geq 2$ and $g_1=1$. In deriving this equation we have used $E_s = \alpha s + \delta$ [see (16)] and defined $\lambda = \exp[\beta(\mu - \alpha)]$ with μ denoting the chemical potential (per unit micelle) of the system; μ enters (22) as the Lagrange multiplier conjugate to (19).

In the limit of ideal solution (of noninteracting rods) the second term in the exponent in (22) vanishes and we recover the usual expression for the size distribution of self-assembling rodlike micelles.^{2,3,32} That is, $\rho_s(x) = \rho_s(y) = \rho_s/2$ with

$$\rho_s = g_s \lambda^s \exp(-\beta\delta) = g_s (\rho_1/g_1)^s \exp[-\beta(E_s - sE_1)]. \quad (23)$$

In this limit the chemical potential is given by the common expression $\beta\mu = \beta\mu_s^0 + (1/s)\ln\rho_s$, with $s\beta\mu_s^0 = -\ln g_s + \beta E_s$ denoting the “standard chemical potential” of an s micelle. (Note that $g_s=2$, for $s \geq 2$, is the orientational degeneracy of the rods.) Using (19), it is not difficult to show that for $\beta\delta \gg 1$, the weight averaged size is given by

$$\langle s \rangle = \frac{\sum s^2 \rho_s}{\sum s \rho_s} \cong \sqrt{4c \exp(\beta\delta) + 1}. \quad (24)$$

For the most probable size, s^* , and the number averaged size $\bar{s} = \sum s \rho_s / \sum \rho_s$ one finds $s^* \approx \bar{s} \approx \langle s \rangle / 2$. Our MC calculations of the size distribution and the average size in dilute solution are, not surprisingly, in excellent agreement with (23) and (24).

To account for intermicellar interactions we have to solve (22). These equations, valid for a system of long rods (where third and higher virial corrections are negligible), cannot be solved exactly even for a monodisperse system. Before commenting on their numerical solution, it should be noted that in dilute (but not ideal) solution we expect that inter-rod interactions will modify the size distribution $\{\rho_s\}$, but not the orientational distribution, i.e., the system remains isotropic $\rho_s(x) = \rho_s(y) = \rho_s/2$. Anisotropic (nematic) solutions, $\rho_s(x) \neq \rho_s(y)$, are only expected at higher concentrations, when $c\langle s \rangle \approx 1$, as noted above.

Since $\Omega = x, y$ is restricted to two orientations the Ω' summation in (22) involves only two terms. We also note that $B_{ss'}(x, x) = B_{ss'}(y, y) = B_{ss'}^{\parallel}$ and $B_{ss'}(x, y) = B_{ss'}(y, x) = B_{ss'}^{\perp}$. Using (21) the “parallel” and “perpendicular” virial coefficients corresponding to our model are found to be (for $\epsilon_n = \epsilon_p$).

$$B_{ss'}^{\parallel} = 2(s + s') - f^{\parallel}(s, s'), \quad (25)$$

$$B_{ss'}^{\perp} = \frac{1}{2}[s s' + 3(s + s') + 1] - f^{\perp}(s, s'). \quad (26)$$

The first terms in each of these two equations correspond to (one half of) the excluded area of the two rods, assuming that the rods, or portions thereof, are not allowed to occupy NN sites. These are the excluded areas corresponding to low temperatures. The second terms in (25), (26) account for two-rod configurations involving NN contacts (excluding two parallel rods touching at their ends, a configuration representing one

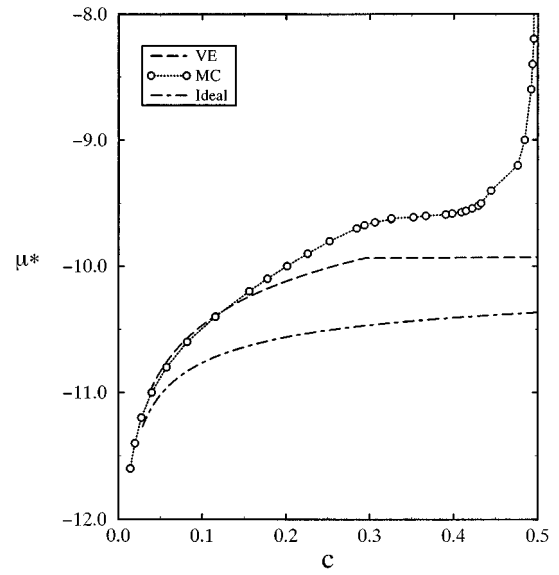


FIG. 13. Three μ - c isotherms, all for the $b=0$, $\gamma=-1.5K^2$ system, at $T^*=0.3$. Shown are the results obtained from grand canonical MC simulations, the virial expansion calculation scheme and, for comparison, an isotherm corresponding to an ideal system. [The ideal system corresponds, formally, to $B_{ss'}(\Omega, \Omega')=0$ in Eq. (20).]

larger rod). The explicit expressions for these functions are: $f^{\parallel}(s, s') = (2 + s + s') - (2p + s + s' - 1)q^{s'} + 2(s' - 1)/(1 - q)$ for $s \geq s' \geq 2$, where $q = \exp(2\beta\epsilon_f)$ and $p = \exp[2\beta(\epsilon_p - \epsilon_f)]$, and $f^{\perp}(s, s') = (s + s' - 4)(q - 1) + 4pq$. Both functions vanish as $|\beta\epsilon_f| \rightarrow 0$, ($\epsilon_p = \epsilon_n < \epsilon_f < 0$).

Equations (22) were solved numerically, using (25) and (26), for the three temperatures considered in Fig. 11. For $T^*=0.45$ and 0.6 we found isotropic solutions, $\rho_s(x) = \rho_s(y)$, up to $c=0.5$. This is not too surprising considering that the average rod length in the system is rather small, e.g., $\langle s \rangle \approx 6$ for $T^*=0.45$ at $c=0.3$. Only at the lowest temperature analyzed, $T^*=0.3$, was an anisotropic solution found, appearing at $c \geq 0.3$. The μ - c isotherm corresponding to this calculation is shown, along with the MC isotherm in Fig. 13. The VE and MC isotherms show good quantitative agreement up to rather high area fractions, $c \leq 0.25$, beyond which point they start diverging. Both calculations indicate a change in the slope of μ at $c = \tilde{c} \approx 0.3$, suggesting a second (or higher) order, isotropic–anisotropic, phase transition. This is consistent with the order parameter calculations in Fig. 12(a), which show a change in η at this value of c . Similarly, the change in slope of the VE curve occurs at the point where an anisotropic solution to (22) first appears. It was found that once an anisotropic solution is a minimum of the free energy, the isotropic solution becomes a maximum, confirming that the transition is of second order.

It is also interesting to compare the size distributions, $P(s)$, obtained from the VE and MC calculations. These are shown in Fig. 14. At the lowest concentration shown, $c=0.25$, the agreement is excellent. At higher concentrations the agreement becomes less and less impressive, as could be expected from the growing difference in the μ vs c plots in Fig. 13. Yet, it should be noted that the overall shape of the distributions is quite similar. Figure 14(b), for instance, shows

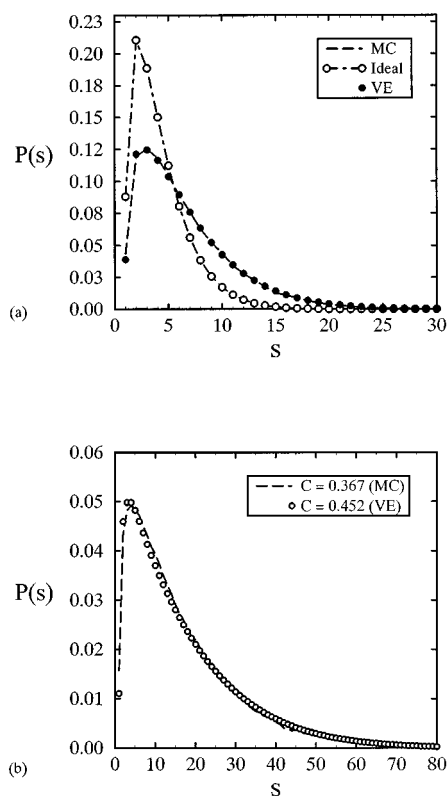


FIG. 14. Micellar size distributions obtained from the VE analysis and MC simulations for the $b=0$, $\gamma=-1.5K^2$ system, at $T^*=0.3$. (a) Both the VE and MC distributions correspond to $c=0.25$, at which concentration the system is still isotropic; (b) MC- and VE-size distributions in the anisotropic phase, corresponding to $c=0.37$ and $c=0.45$, respectively.

size distributions at high concentrations, when the system is already in the anisotropic phase. We see that the size distribution derived from the MC simulations for $c=0.37$ nearly overlaps the one obtained from the VE calculation at a somewhat higher concentration, $c=0.45$. Both the MC and the VE calculations show a rapid increase in the average rod size once orientational order sets in. This “alignment induced growth” in the nematic (or, more precisely, stripe) phase had been suggested by earlier lattice¹³ and virial expansion^{14–16} treatments of the isotropic–nematic transition in 3D self-assembling systems.

From the VE calculations we have also evaluated the orientational order parameter in the nematic phase as a function of the rod size. We find that the longer rods are more strongly aligned, and the degree of alignment increases with concentration. Qualitatively similar behavior was found in virial expansion treatments of the isotropic–nematic transition in 3D self-assembling systems.¹⁴

D. Transition order

It is well known that in 3D systems of rodlike particles the isotropic–nematic transition is of first order.³³ This has been shown to be the case for a variety of models and systems, including systems governed by attractive and/or repulsive interactions, for lattice and restricted orientation models of monodisperse systems, as well as for polydisperse and self-assembling systems.³⁴ In monodisperse 2D systems the

transition is most likely of second order. This has been concluded to be the case based on a virial expansion (up to seventh order) of the free energy in a monodisperse system of rods which, as in our system, are restricted to only two allowed orientations.³⁵ A similar result follows also from a Landau-type expansion of the free energy corresponding to the *second* virial approximation.³⁶ We briefly outline this analysis because of its relevance to our present calculations.

Consider a monodisperse system of rods, all of size (axial ratio) χ . The rods are restricted to two allowed orientations, along either the x or the y directions. Introducing the orientational order parameter η , defined as $\rho(x)/\rho=1/2+\eta$, $\rho(y)/\rho=1/2-\eta$, [$\rho=\rho(x)+\rho(y)$], we can express the second virial free energy per rod, $\varphi=F/(M\rho)$, as

$$\beta\varphi = \left(\frac{1}{2} + \eta\right) \ln\left(\frac{1}{2} + \eta\right) + \left(\frac{1}{2} - \eta\right) \ln\left(\frac{1}{2} - \eta\right) - 2\eta^2\rho\Delta B + \text{const.} \quad (27)$$

The constant terms here depend on ρ but not on η . Also $\Delta B \equiv B^\perp - B^\parallel$ where $B^\perp = B(x,y) = B(y,x)$ and $B^\parallel = B(x,x) = B(y,y)$.

Minimization of φ with respect to η yields [in analogy to (22)]

$$\ln\left(\frac{1+2\eta}{1-2\eta}\right) = 4\eta\rho\Delta B. \quad (28)$$

The isotropic solution, $\eta=0$, is always a solution of this equation. It is a minimum, i.e., the equilibrium solution, for densities ρ lower than a critical density ρ_c . At $\rho \geq \rho_c$ the minimum of φ corresponds to the anisotropic solutions $|\eta| \neq 0$, with $|\eta|$ increasing continuously from $\eta=0$, the isotropic solution eventually becoming a maximum. The critical density is found from $\partial^2\varphi/\partial\eta^2=0$ (at $\eta=0$), yielding

$$\rho_c = 1/\Delta B. \quad (29)$$

The variation of the order parameter with respect to ρ in the anisotropic phase, near the transition point, is given by

$$\eta = \pm \left(\frac{\sqrt{3}}{2}\right) \sqrt{\frac{\rho}{\rho_c} - 1}. \quad (30)$$

Using (25), (26) with $\chi=s=s'$, we find (neglecting the f^\parallel, f^\perp corrections) $\Delta B = (\chi-1)^2/2$ and hence $\rho_c = 2/(\chi-1)^2$. The critical area fraction c_c is thus given by $c_c = 2\chi/(\chi-1)^2 \sim 2/\chi$. Estimating χ for our self-assembling system as $\chi \sim \langle s \rangle \approx 2\sqrt{c} \exp(\beta\delta)$ we find $c_c \sim \exp(-\beta\delta/3) = \exp(-1/2T^*)$ (the last equality holds for $\delta=K^2$), as we found earlier for $\tilde{c} \approx c_c$ based on simpler considerations.

E. LG analysis

The virial expansion treatment detailed above is applicable at low temperatures where the micelles are predominantly rodlike. This treatment analyzes the appearance of *orientational* order in the system. In Figs. 9 and 10 we clearly note a stripelike *positional* order around $c=0.5$, which at low T appears only after orientational order has set in. The LG theory mentioned in Sec. II is applicable at all

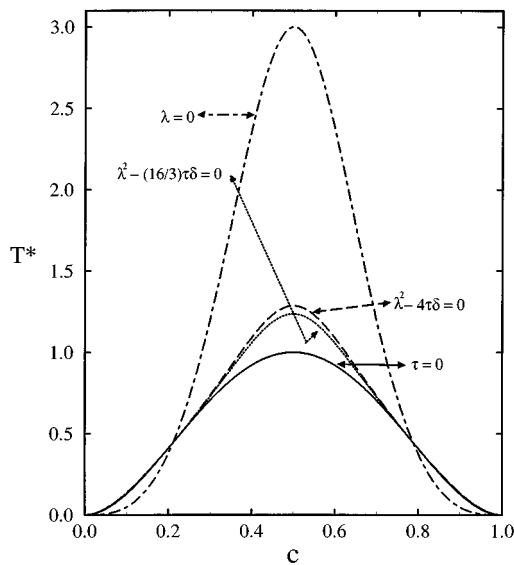


FIG. 15. The Landau–Ginzburg phase diagram for the system $b=0$, $\gamma=-1.5K^2$. The solid and dashed curves mark the stability limits of the isotropic and stripe phases, respectively. Along the dotted curve the free energies of the two phases are equal. Above $T^*=0.44$ the transition is of first order, below this temperature it is of second order.

temperatures. It should be noted, however, that since it is only concerned with the establishment of positional order, it should be regarded as a complementary approach rather than an alternative to our VE treatment. The application of the LG scheme to our 2D lattice model has been described in detail in Ref. 1. Here we shall only briefly outline its predictions for the system $b=0$, $\gamma/K^2=-1.5$.

The LG free energy, per unit area, is given by (5), with e denoting the amplitude of a stripe phase characterized by a density modulation along, say, the x axis, $c(\mathbf{r})=2e \cos(kx)$. Based on considerations detailed in Ref. 1, it can be shown that for $b=0$, $\gamma=-1.5K^2$ the optimal (minimum free energy) stripe modulation corresponds to $k=\pi$, i.e., alternating occupied and vacant stripes, as in Fig. 9(c). For these model parameters it is also found that the coefficients τ , λ , and δ in (5) are given by

$$\tau=2T^*/c(1-c)-32c(1-c), \quad (31)$$

$$\lambda=2T^*[1/(1-c)^3+1/c^3]-96, \quad (32)$$

$$\delta=4T^*[1/(1-c)^5+1/c^5], \quad (33)$$

with all energies (i.e., f, τ, λ, δ) measured in units of K^2 . These expressions, together with f_0 from (4) are now inserted into (5), yielding an explicit expression for f in terms of c , T^* and the order parameter e .

The extrema of f with respect to e correspond to an isotropic phase, $e=0$ and $f=f_0$, and a stripe phase with order parameter $e^2 = -(\lambda/2\delta)[1 + \sqrt{1-4\tau\delta/\lambda^2}]$ and free energy $f_s=f_s(e)$. The curve $\tau=(\partial^2 f/\partial e^2)_{e=0}=0$ marks the local stability limit of the isotropic phase; this yields $T^*=16c^2(1-c)^2$, see Fig. 15. For $c=1/2$ this implies $T=T_0^*=1$. If upon lowering T^* at a given c , the coefficient τ changes sign from positive to negative while λ is still positive the transition is of second order. If, on the other hand, λ

becomes negative while τ is still positive, the transition is of first order, describing a discontinuous jump in e from 0 to a finite value. In order that e^2 will be real it is required that in addition to being negative, λ should also satisfy $4\tau\delta/\lambda^2 \leq 1$. This condition marks the local stability limit of the stripe phase; for $c=1/2$ it yields $T=T_s^*=9/7$, Fig. 15.

The curves corresponding to the stability limits of the isotropic and stripe phases cross each other when $\tau(c, T)=\lambda(c, T)=0$. The solution of these equations marks a tricritical point. For the system considered in this section we find two such points, symmetrically located around $c=0.5$ (because of the particle–hole symmetry), namely, at $c_{tc}=0.22$, $T_{tc}^*=0.44$ and $c_{tc}=0.78$, $T_{tc}^*=0.44$. The curve $f_0=f_s$, along which the free energies of the isotropic and stripe phases are equal, also passes through the tricritical points. From the LG expression for the free energy it follows that $f_0=f_s$ implies $16\tau\lambda/3\lambda^2=1$. This last equality yields a T^* vs c curve reaching a maximum of $T^*=1.24$ at $c=0.5$. From these calculations one concludes that a second-order transition from an isotropic to a stripe-modulated phase should take place at low temperatures ($0 \leq T^* \leq 0.44$), whereas at higher temperatures ($0.44 \leq T^* \leq 1.24$) the transition is of first order.

A direct comparison of the LG analysis with our other calculations is not simple, at least not at low T where an isotropic–nematic ($I-N$) transition also takes place. The simulations indicate that the stripe phase develops from the nematic phase (as “alignment induced growth”). On the other hand, at (relatively) high T the stripe order develops directly from the isotropic phase. At these temperatures the LG analysis predicts a first-order transition whereas the MC results suggest a continuous transition. Yet it must be stated that the analysis of the MC calculations is not sufficiently detailed to discern between a “strong second-order” and a “weak first-order” transition.

V. MICELLAR JUNCTIONS AND NETWORKS

In Secs. III and IV we have considered systems composed of micelles with positive ($b=K>0$) and zero ($b=0$) spontaneous rim curvature. We now turn to systems with $b<0$ which implies low ϵ_n , i.e., favoring the negative rim curvature [see (2)]. In the high concentration (bilayer) regime, lowering the energy of a “negatively curved” rim enhances the formation of *hole defects*. In dilute solution $b<0$ implies low (possibly even negative) free energy change when linear micelles associate to form *branched aggregates*. Upon increasing the concentration these micelles can associate into a network (“gel”) which may, or may not, separate as a condensed phase coexisting with a dilute micellar solution. The exact scenario of the phase evolution depends on the delicate balance between the energy parameters ϵ_p , ϵ_n , ϵ_f , and ϵ_b which, in turn, depend on the line tension γ , the bending rigidity K , and the spontaneous curvature b . Similar complex behavior, reflecting the intricate interplay between molecular packing energies in different micellar microenvironments, characterizes the phase evolution in real surfactant solutions.

The model systems considered in this section have been

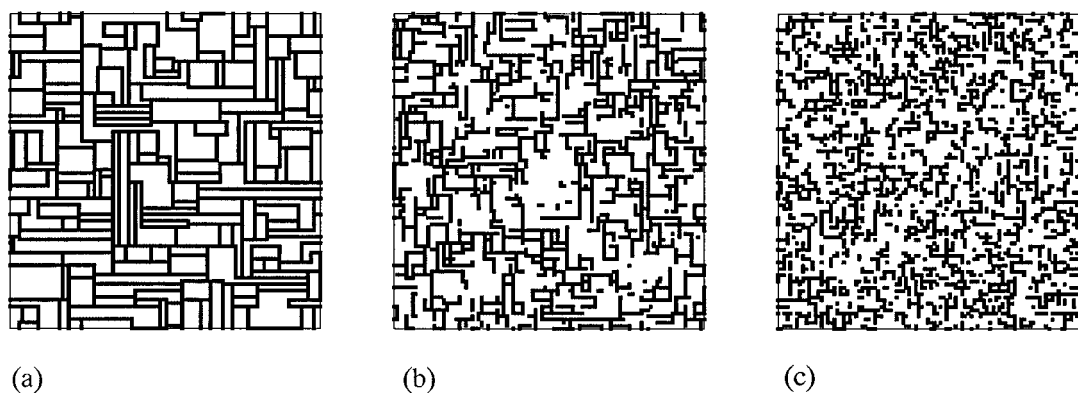


FIG. 16. Typical MC snapshots for the case $b = -K$, $\gamma = -4K^2$. The configurations shown correspond to the same concentration, $c = 0.3$, but the temperatures are different: $T^* = 0.1, 1.0$ and 2.0 for a, b , and c , respectively. At the lowest temperature here (a) a stable 2D network of linear micelles spans the entire system, as discussed in Sec. V B, case (i). Upon raising the temperature bonds in the network break up (b) leading eventually to the formation of an isotropic phase of small, bent and branched, micelles (c).

chosen in order to demonstrate the possible formation of branched micelles and networks by “controlling” the preferred spontaneous curvature and bending rigidity. The existence of such structures and phases which, until recently, had not been considered as a likely possibility, is now evidenced by both direct^{23,24} and indirect experimental methods.^{19–21} Porte suggested²⁵ that their appearance requires special ambient conditions (added salt or cosurfactant) which favor the formation of *junctions* between cylindrical micelles. This is because the local packing geometry at the junctions is saddlelike and requires rather special values of the spontaneous curvature. In our 2D model, junctions will form when $b < 0$ and $\gamma < 0$. Due to the low symmetry of the square lattice the junctions are necessarily T-like. Notwithstanding these provisos our calculations strongly support the suggestion that branched micelles and networks are indeed possible.

A. MC simulations

Given that both b and γ are negative many γ, b, K combinations can give rise to branched micelle formation in di-

lute solution and their association into networks upon increasing the concentration. We have chosen to present here two sets of simulations, both correspond to $\epsilon_n < \epsilon_f < \epsilon_p = \epsilon_b = 0$. Explicitly, for one system, hereafter (i): $\gamma/K^2 = -4$, $b = -K$ implying $\epsilon_n/K^2 = -4$, $\epsilon_f/K^2 = -3$, $\epsilon_p = 0$. The parameters corresponding to system (ii) are: $\gamma/K^2 = -9$, $b = -2K$ implying $\epsilon_n/K^2 = -8$, $\epsilon_f/K^2 = -5$, $\epsilon_p = 0$. In Figs. 16 and 17, we show two sets of c, M, T simulation snapshots. Both sets describe the structural evolution of the system at constant concentration ($c = 0.3$) upon raising the (reduced) temperature $T^* = kT/K^2$.

The systems described in Figs. 16 and 17 differ only in the relative magnitudes of ϵ_n and ϵ_f , yet this difference implies a qualitatively different phase behavior upon lowering T^* . In the first case, Fig. 16, the system is isotropic at high temperatures, containing bent and branched isolated micelles. As T^* decreases the micelles associate into larger aggregates, thereby gradually getting rid of the unfavorable end cap energy (ϵ_p is large compared to ϵ_f, ϵ_n). No free ends

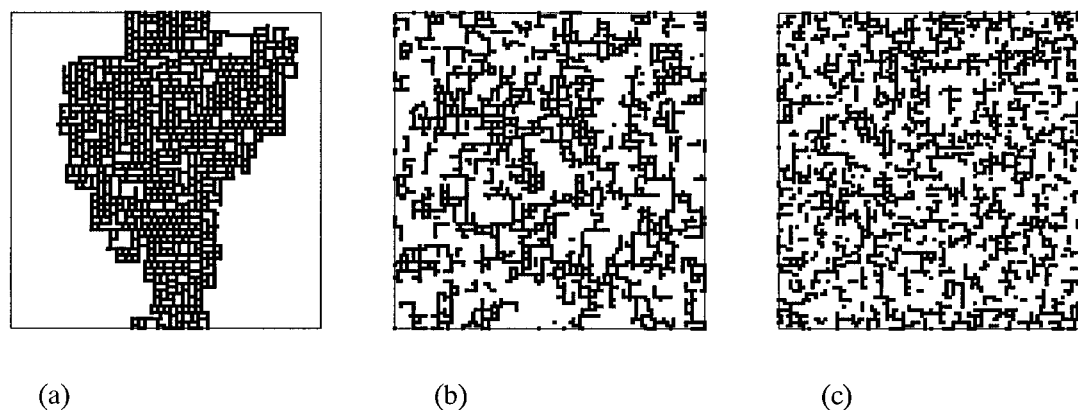


FIG. 17. Typical MC snapshots for the $b = -2K$, $\gamma = -9K^2$ system, all for concentration $c = 0.3$, but the temperatures are different: $T^* = 1.0, 2.0$ and 3.0 for a, b , and c , respectively. At high temperatures the system consists of isolated (branched, bent and even some looplike) micelles (c). As T is lowered the micelles associate into larger aggregates (b) containing both large and small micellar loops. At the lowest temperature here (a), a network consisting of small loops forms a separate phase which coexists with a dilute micellar phase.

are left at the lowest T^* considered, where a connected network of linear micelles spans over the entire lattice. A different phase evolution is observed when $\gamma/K^2 = -9$, see Fig. 17. Here, again, at high T^* the system contains finite branched micelles, but we also note the appearance of “loops.” Upon lowering T^* the loops (or “holes”) associate into a dense network coexisting with an extremely dilute micellar solution.

The formation of loops is not surprising since each loop involves (at least four) energetically favorable ϵ_n 's. While this is true for both systems shown, only one system exhibits macroscopic phase separation; the other equilibrates (at low T^*) by forming a uniform network which spans the entire lattice, with a mesh size depending on the overall concentration c (see below). We also note that in both cases, upon lowering T^* (or increasing c), the condensed phase formed is isotropic, as opposed to the formation of the stripe phase characterizing the $b=0$ system considered in the previous section.

In our model, the appearance of branched micelles and networks of linear (rigid or flexible) micelles requires that the energetic change associated with the fusion of two rod-like micelles into a T-like micelle is negative, i.e., $\Delta E_T = 2\epsilon_n - 2(\epsilon_f + \epsilon_p) = -2\gamma - 2(b^2 - 4bK) < 0$. For the systems considered in Figs. 16 and 17 we find $\Delta E_T = -2K^2$ and $-6K^2$, respectively. Not surprisingly, ΔE_T is considerably lower for the latter system, reflecting its stronger tendency to form junctions and loops.

The free energy change, ΔF , involved in the association of rigid (rodlike) and flexible (wormlike) micelles into connected networks was estimated by Drye and Cates²² based on mean-field and scaling arguments. The energetic contribution was calculated by considering the energy change involved in the association of free end caps to form a junction of a given functionality (coordination number). The entropy change involves replacing the translational freedom of the micelles by the (restricted) translational motion of the junctions in the network. It was shown that the network can be “saturated” or “unsaturated” depending on the energetic and entropic contributions to the free energy. Unfortunately, testing this theory for our model is not straightforward, primarily because this model is two dimensional and hence, for instance, cannot distinguish between entanglements and junctions. Thus in the remainder of this section we present an alternative, qualitative and approximate, analysis, attempting mainly to explain the different behaviors characterizing the two systems considered in Figs. 16 and 17.

B. Network stability

Suppose the unit micelles constituting the system have organized into an isotropic network of linear micelles, as shown in Fig. 16(a). Let L denote the average mesh size, i.e., the average length of a rodlike segment connecting two branched points. We assume that the thickness of the linear segments is one lattice unit, and that there are no free end caps. To relate L to the concentration, c , suppose the network is composed of rectangular loops. We then find $c = (2L - 1)/L^2$. The number of loops per unit area is $1/L^2$.

Taking, as usual, the perfect bilayer as a reference for calculating the energy, the average energy per loop is $4\epsilon_n + 4(L - 2)\epsilon_f$.

The network entropy can be estimated by regarding it as composed of segments (or loops, or sides of rectangles) of different lengths, l , with size distribution $P(l)$ satisfying $\sum lP(l) = L$. (Note that the most condensed network corresponds to $l=2$, hence in all sums $l \geq 2$) For a given c , and hence a given L , the entropy of the system is proportional to the average entropy per segment $-\sum P(l)\ln P(l)$. Maximizing this expression subject to $\sum lP(l) = L$ it can be shown that the entropy, per loop, is given by

$$s = \frac{1}{2}k\{\ln(L-2) + (L-1)\ln[(L-1)/(L-2)]\}. \quad (34)$$

This actually is an upper bound to the entropy, since we ignored correlations between different segments. (A better estimate of the entropy, which corrects for the fact that the rod segments are joined at the junction points is given in Ref. 22.) A lower bound on s may be obtained by assuming that each segment can be freely moved over $\sim(L-1)$ positions corresponding, on the average, to the distance between two neighboring segments. This yields, per loop

$$s = k \ln(L-1). \quad (35)$$

Note that both estimates give $s=0$ for the “minimal” loop size, $L=2$, ($c=0.75$). It turns out that for the systems considered in this section the qualitative conclusions from the stability analysis which follows, are the same for both (upper and lower bound) estimates of the entropy. We shall thus employ the simpler one (35).

Using (35) for s we find that the free energy, per unit area, is given by

$$\beta f = \frac{4\beta}{L^2} [\epsilon_n + (L-2)\epsilon_f] - \frac{2}{L^2} \ln(L-1). \quad (36)$$

The chemical potential $\mu = \partial f / \partial c = -[L^3/2(L-1)]\partial f / \partial l$ is

$$\beta\mu = \frac{1}{L-1} \left\{ 2\beta[\epsilon_n + (L-4)\epsilon_f] - 2 \ln(L-1) + \frac{L}{L-1} \right\} \quad (37)$$

and the stability condition, $\partial\mu/\partial c \geq 0$, becomes

$$\beta(2\epsilon_n - 3\epsilon_f) - \ln(L-1) + \frac{3L-1}{2(L-1)} \geq 0. \quad (38)$$

At low concentrations $L \sim 2/c$ is large and a stable network can only exist if $\beta(2\epsilon_n - 3\epsilon_f) > 0$. For the two special cases considered in this section we have: (i) $\beta(2\epsilon_n - 3\epsilon_f) = 1/T^*$ for the system in Fig. 16, and (ii) $\beta(2\epsilon_n - 3\epsilon_f) = -1/T^*$, for the systems in Fig. 17. For the first system we indeed find a stable uniform network at $T^* \geq 2$, with $L \sim 7$. On the other hand the second system is unstable; the network shrinks to a smaller size ($L \approx 3-4$) and coexists with a very dilute micellar phase. The concentration of the micellar phase, c' , can be estimated by comparing its chemical potential to that of a network, (37). Since c' is extremely small it can safely be assumed that the dilute phase contains only unit micelles, whose self-energy is $4\epsilon_p$. Thus, its chemical potential is $\beta\mu = 4\beta\epsilon_p + \ln c'$. Using (37) with, say, $L=4$, and with the energy parameters corresponding to system (ii), namely,

$\beta\epsilon_n = -8/T^*$, $\beta\epsilon_f = -5/T^*$, $\epsilon_p = 0$, we find $\ln c' \approx -5/T^*$. This explains the vanishingly small concentration of micelles in the dilute phase which, on the scale of our simulations appears as an empty region of space.

Since f , as given by (36) corresponds to the free energy of a network of mesh size L , our crude stability analysis only indicates if the system is stable against phase separation into dilute ($L' > L$) and concentrated ($L' < L$) networks. However, a dilute phase is more likely to consist of isolated (rather than connected) micelles. This is the reason for comparing, in the last stage of the analysis above, the free energy of the network to that of a dilute micellar phase. A more complete stability analysis would require consideration of other possible phases, e.g., concentrated nematic or stripe phases. Indeed, simple energetic and entropic considerations can be used to explain the higher stability of the network compared, say, to that of a stripe phase (when $\epsilon_n < \epsilon_f$), as found in our simulations.

VI. CONCLUDING REMARKS

In this paper we have focused on various scenarios for the evolution of micellar structure and long-range order in two-dimensional systems of surfactants in water. Our initial motivation came from the x-ray/NMR investigations by Holmes and Charvolin⁶ of possible percolation from micellar disks and ribbons to continuous bilayer in decylammonium chloride/water/ammonium chloride (DACl/ACl) solutions, and from reports of smectic-*A* phases of disklike micelles, reported by Boden *et al.*²⁶ for cesium pentadecafluorooctanoate/water solutions and by Zasadzinski and co-workers (including cryo-electron microscopy studies), again for the DACl/ACl system.²⁷ In all of these cases, it is significant that the changes in micellar morphology, and the onset of positional ordering, essentially occur within the individual layers of lamellarlike/smectic phases. Accordingly, we have argued that it is appropriate to model these phenomena via a two-dimensional statistical mechanical theory. Insofar as we need to account for evolving size and shape of micelles—e.g., from small disks to bigger ones or to extended, ribbonlike structures—and simultaneously for their long-range order or percolation into (2D) space-filling bilayers, we have found it natural and useful to employ a lattice-gas model. The elementary “particle” in our model is the small-disk micelle which dominates the isotropic and nematic phases preceding the layered state. When it fuses to form bigger disks or ribbons there is an energy change associated with the fact that molecules in the rim of the disk have been “converted” into ones in a bilayer environment. These energy changes are described by two-, three-, and four-site interaction terms in the lattice gas hamiltonian, whose coefficients are related to the preference for optimally curved rim over bilayer and—more generally—to the curvature elasticity properties of the surfactant, specifically the spontaneous curvature and bending energy. The statistical mechanical phase behavior associated with this Hamiltonian is then determined by a variety of analytical techniques, including simple mean-field, Landau–Ginzburg, and Bethe–Peierls ap-

proximations, as well as by Monte Carlo simulations, the latter two sets of results agreeing quite closely with one another.

We have concentrated on essentially two different scenarios of micellar structural evolution and phase behavior. In the first, the optimum rim curvature corresponds to small disks being favored; here we find a transition from disordered disks to continuous bilayer, with the possibility of an intermediate phase in which the density of disks shows a modulated (“checkerboard”) spatial structure. On the other hand, when the rim is sufficiently lower in energy than the bilayer, and specifically when its spontaneous curvature vanishes, then extended ribbonlike micelles are strongly preferred. In this scenario we pursue two quite different cases: one where straight micelles are dominant; and the other where branched ones appear, involving T-like junctions. The first case is shown to give rise to a progression from isotropic to nematic to “stripe” phases, with average aggregation number increasing dramatically upon increase in surfactant concentration. The second suggests an evolution from isolated branched micelles in dilute solution to various kinds of space-filling network structures at high concentrations and low temperature, scenarios which are now beginning to be observable in experimental studies.

ACKNOWLEDGMENTS

We are grateful to Gregoire Porte for many illuminating discussions on intermicellar junctions and networks. We thank Mats Almgren and Ishi Talmon for sending us their electron micrographs of branched micelles, prior to publication. We also thank Jean Candau and Raoul Zana for helpful discussions concerning their work on branched micellar systems. Y.B. thanks Alia for her patience. This work was completed while A.B.-S. was a Ludwig Schaffer visiting scholar at the department of Molecular Biophysics of Columbia University, New York. He would like to thank Professor Barry Honig for his hospitality during this period. A.B.-S. acknowledges the Yeshaya Horowitz Association for funding this work. W.M.G. would like to thank the National Science Foundation, through Grant No. CHE-92-01166 for partial financial support. The Fritz Haber Research Center is supported by the Minerva foundation, Munich, Germany. R.G. is an incumbent of the William T. Hogan and Winifred T. Hogan Career Development Chair.

¹R. Granek, W. M. Gelbart, Y. Bohbot, and A. Ben-Shaul, *J. Chem. Phys.* **101**, 4331 (1994).

²For a most recent general introduction to the statistical thermodynamics and experimental measurements of structure and phase behavior in micellized surfactant solutions, see *Micelles, Membranes, Microemulsions, and Monolayers*, edited by W. M. Gelbart, A. Ben-Shaul, and D. Roux (Springer-Verlag, New York, 1994), especially Chaps. 1–3.

³J. N. Israelachvili, D. J. Mitchell, and B. W. Ninham, *J. Chem. Soc. Faraday Trans. 2* **72**, 1525 (1976).

⁴H. Wennerstrom and B. Lindman, *Phys. Rep.* **52**, 1 (1979).

⁵S. S. Funari, M. C. Holmes, and G. J. T. Tiddy, *J. Phys. Chem.* **98**, 3015 (1994).

⁶M. C. Holmes and J. Charvolin, *J. Phys. Chem.* **88**, 810 (1984).

⁷P. O. Quist, K. Fontell, and B. Halle, *Liq. Cryst.* **16**, 235 (1994).

⁸C. K. Bagdassarian, D. Roux, A. Ben-Shaul, and W. M. Gelbart, *J. Chem. Phys.* **94**, 3030 (1991).

⁹M. P. Taylor, A. E. Berger, and J. Herzfeld, *J. Chem. Phys.* **91**, 528 (1989);

- see also M. P. Taylor and J. Herzfeld, *J. Phys.: Condens. Matter* **5**, 2651 (1993).
- ¹⁰M. P. Taylor and J. Herzfeld, *Phys. Rev. A* **43**, 1892 (1991).
- ¹¹G. Porte, Chap. 2 in Ref. 2 and papers cited therein.
- ¹²See for example, P. J. Missell, N. A. Mazer, G. B. Benedek, C. Y. Young, and M. C. Carey, *J. Phys. Chem.* **84**, 1044 (1980); G. Porte and J. Appell, *ibid.* **85**, 2511 (1981).
- ¹³J. Herzfeld and R. W. Briehl, *Macromolecules* **14**, 397 (1981).
- ¹⁴W. E. McMullen, W. M. Gelbart, and A. Ben-Shaul, *J. Chem. Phys.* **82**, 5616 (1985).
- ¹⁵T. Odijk, *J. Physique* **48**, 125 (1987).
- ¹⁶P. van der Shoot and M. E. Cates, *Langmuir* **10**, 670 (1994).
- ¹⁷See for example, S. J. Candau, E. Hirsch, and R. Zana, *J. Coll. Interf. Sci.* **105**, 521 (1985).
- ¹⁸M. E. Cates, *Macromolecules* **20**, 2289 (1987); *J. Phys. Chem.* **94**, 371 (1990); see also M. E. Cates and S. J. Candau, *J. Phys.: Condensed Matter* **2**, 6869 (1990).
- ¹⁹The possible formation of branched ("cross linked") micelles was first conjectured by G. Porte, R. Gomati, O. El Hataimy, J. Appell, and J. Marignan, *J. Phys. Chem.* **90**, 5746 (1986). See also J. Appell, G. Porte, A. Khatory, F. Kern and J. S. Candau, *J. Phys. II France* **2**, 1045 (1992); A. Khatory, F. Kern, F. Lequeux, J. Appell, G. Porte, N. Morie, A. Ott, and W. Urbach, *Langmuir* **9**, 933 (1993).
- ²⁰S. J. Candau, A. Khatory, F. Lequeux, and F. Kern, *J. Physique IV. Colloque C1* **3**, 197 (1993); F. Kern, F. Lequeux, R. Zana, and S. J. Candau, *Langmuir* **10**, 1714 (1994); A. Khatory, F. Lequeux, F. Kern, and S. J. Candau, *ibid.* **9**, 1456 (1993); F. Lequeux and S. J. Candau, *Structure and Flow in Surfactant Solutions*, Am. Chem. Soc. Symp. Series No. 578, edited by C. Herb and R. Prud'homme, Am. Chem. Soc. 51 (1994); F. Lequeux, *Europhys. Lett.* **19**, 675 (1992).
- ²¹Structures resembling branched micelles were reported in a recent molecular dynamics study, see S. Karaborni, K. Esselink, P. A. J. Hilbers, B. Smit, J. Karthaus, N. M. van Os, and R. Zana, *Science* **266**, 254 (1994).
- ²²T. J. Drye and M. E. Cates, *J. Chem. Phys.* **96**, 1367 (1991).
- ²³M. Almgren, personal communication.
- ²⁴D. Danino, Y. Talmon, H. Levy, G. Beinert, and R. Zana, *Science* (in press); Y. Talmon, personal communication.
- ²⁵G. Porte, personal communication.
- ²⁶N. Boden, S. A. Corne, and K. W. Jolley, *J. Phys. Chem.* **91**, 4092 (1987); N. Boden, R. J. Bushby, K. W. Jolley, M. C. Holmes, and F. Sixl, *Mol. Cryst. Liq. Cryst.* **152**, 37 (1987); N. Boden, Chap. 3 in Ref. 2.
- ²⁷M. J. Sammon, J. A. N. Zasadzinski, and M. R. Kuzma, *Phys. Rev. Lett.* **57**, 2834 (1986); J. A. N. Zasadzinski, M. J. Sammon, and M. R. Kuzma, in *Ordering and Organization in Ionic Solutions*, edited by N. Ise and I. Sogami (World Science, Singapore, 1988).
- ²⁸J. Israelachvili, *Langmuir* **10**, 3774 (1994).
- ²⁹See for example, T. L. Hill, *Statistical Mechanics: Principles and Selected Applications*. (Dover, New York, 1956).
- ³⁰See for example, D. L. Adams, *Surf. Sci.* **42**, 12 (1974).
- ³¹D. Stauffer, *Introduction to Percolation Theory* (Taylor and Francis, London, 1985).
- ³²A. Ben-Shaul and W. M. Gelbart, Chap. 1 in Ref. 2.
- ³³L. Onsager, *Ann. NY Acad. Sci.* **51**, 627 (1949).
- ³⁴For a review see e.g., W. M. Gelbart, *J. Phys. Chem.* **86**, 4298 (1982).
- ³⁵R. Zwanzig, *J. Chem. Phys.* **39**, 1714 (1963).
- ³⁶D. Kramer, A. Ben-Shaul, Z.-Y. Chen, and W. M. Gelbart, *J. Chem. Phys.* **96**, 2236 (1992).